TAMPEREEN TEKNILLINEN YLIOPISTO
TAMPERE UNIVERSITY OF TECHNOLOGY

PAUL OCTAVIAN BOLCOS

EVALUATION OF MIXING EFFICIENCY IN A MICROFLUIDIC CARTRIDGE USING A FINITE ELEMENT METHOD APPROACH

Master of Science thesis

Examiner: Prof. Pasi Kallio
Examiner and topic approved by the Faculty Council of the Faculty of Natural Sciences
on 12th August 2015

ABSTRACT

Paul Octavian Bolcos: EVALUATION OF MIXING EFFICIENCY IN A MICRO-FLUIDIC CARTRIDGE USING A FINITE ELEMENT METHOD APPROACH
Tampere University of technology
Master of Science Thesis, 60 pages, 11 Appendix pages
June 2015
Master's Degree Program in Science and Bioengineering
Major: Biomeasurements
Examiner: Professor Pasi Kallio

Keywords: Microfluidics, Finite Element Method, Modeling, Micromixers, Point-of-care diagnostics

In-vitro diagnostics has shifted from using laboratories to analyze samples, to Point-of-Care devices. These devices offer rapid, near-to-patient analysis, either at the patient's home or the doctor's office. Most Point-of-Care devices use microfluidic principles, since they use small volumes of fluids, handled by microscale channels. When comparing the Point-of-Care devices to conventional testing methods, they benefit from a much smaller reagent consumption, but suffer when it comes to sensitivity and detection limit.

The objective of this research was to study how the mixing performance of a microfluidic immunoassay cartridge can be enhanced. For this purpose, several micromixer geometries, from literature, were studied using a finite element method approach, which was used to characterize and optimize the system.

The mixing efficiency of these micromixer was evaluated by measuring the relative concentration variance of the structures at the outlet against the one inlet, a measure which has also been used in other studies. After the most effective structure was identified, the impact of various parameters, such as pressure, channel length, element width and height, were studied using the same methods. For selecting a micromixer design, along with the mixing efficiency, other parameters were taken into account. These parameters were the probability of air droplet formation, which heavily affects the immunoassay performance, and the manufacturing complexity, which directly impacts the cost of the cartridge.

The results of the simulations showed that a slanted rip micromixer, with an element height of 0.25 mm, element width 1 mm, a channel length of 40 mm, was best suited for this application. The experimental validation, conducted on injection molded polystyrene cartridges, confirmed the mixing behavior predicted in the simulations. Additionally, it revealed that air droplets were rarely formed when blood plasma was flowed through the cartridge.

The approach used in this work is often used when studying micromixer geometries. However, there currently are no studies which investigate the parameter configuration of the slanted rips micromixer and their influence on the mixing efficiency. Moreover, most of the chaotic advection micromixers from literature study the micromixer as a standalone component, rather than in an assembly. In this work, factors influencing the performance of other cartridge components are taken into account.

PREFACE

This thesis was done at the Tampere University of Technology (TUT), in the department of Automation Science and Engineering in 2012-2014. The development of the micro-mixers was part of the Ready-to-use Microfluidic Cartridges for Affordable Point-of-Care Diagnostics project, shortly ReDia project, funded by TEKES.

I would like to thank my supervisor Professor Pasi Kallio for giving me the opportunity to conduct this research with full funding. I am grateful for his patience during the time it took to finalize the thesis and for his guidance and advice given for the research and thesis. I would also like to thank the whole Micro- and Nanosystems research group for providing a pleasurable working environment.

In addition, I would like to thank Rokon Udin for helping me to get started with the research, Jari Väliaho for helping me with modeling and simulations, Joose Kreutzer and Mathias von Essen for advising me with the various practical experiments. Also, thanks to Jyri Öhrling and other from the Polymer laboratory of TUT for injection molding the cartridges, as well as, Ville Hautala and Ari Stjern from the department of Production Engineering of TUT for laser welding the cartridges.

Thanks to my family and friends for the support during the thesis. Also, special thanks to Defne Us for proofreading the thesis and supporting me.

Tampere, October 12th, 2015

CONTENTS

LIST OF FIGURES

LIST OF SYMBOLS AND ABBREVIATIONS

Symbols

CAD	Computer Aided Design
CCD	Charge Coupled Device
cTnI	Cardiac troponin I
DI-water	De-Ionized water
EOS	Equations of State
Eu	Europium
FEM	Finite Element Modeling
IVD	In-Vitro Diagnostics
LOC	Lab-on-a-Chip
NS	Navier-Stokes
PDEs	Partial Differential Equations
PIV	Particle Image Velocimetry
POC	Point of Care
POCT	Point of Care Testing
PS	Polystyrene
TUT	Tampere University of Technology
UDSC	University of Delhi
UTU	University of Turku
UV	Ultraviolet

Abbreviations

a	Circle radius
A	Cross section area
C	Cross section, yz direction
∂C	Boundary, yz direction
C_α	Concentration of solute α, mass fraction
c_α	Concentration of solute α, molecules per volume
c_0	Concentration variance, initial
c_{inlet}	Concentration variance, inlet
c_{outlet}	Concentration variance, outlet
c_p	Concentration of particle p
C_p	Specific heat
d	Mixing length
D	Diffusion coefficient
D_α	Diffusion coefficient of solute α
D_{hyd}	Hydraulic diameter
d_p	Particle diameter
E	Electrical force vector
f	Disturbance frequency
F	Force, drag
G	Gibbs free energy
g	Gravity
h	Height
k	Conduction coefficient
L	Length
m	Mass
m_p	Mass particle

N	Particle number
w	Width
p	Pressure field
Δp	Pressure difference
$\Delta p_{channel}$	Pressure drop over channel
$\Delta p_{capillary}$	Pressure drop due to capillary forces
$\Delta p_{friction}$	Pressure drop due to friction forces
P	Wetted perimeter
Pe	Peclet number
q_{el}	Change density
Q	Volumetric flow rate
Q_m	Mass flow rate
R	Reaction rate
Re	Reynolds number
R_{hyd}	Hydraulic resistance
S	Mixing efficiency measure
St	Strouhal number
T	Temperature
β	Dimensionless viscosity ratio
v	Fluid velocity vector
V	Volume
θ	Contact angle
θ_a	Contact angle, advancing meniscus
θ_r	Contact angle, receding meniscus
γ	Surface tension
γ_{AB}	Surface tension between surfaces A and B
η	Dynamic viscosity
η_i	Dynamic viscosity of fluid i
ρ	Density
τ_{diff}	Average diffusion time
τ_{conv}	Average convection time

1. INTRODUCTION

1.1 ReDia Project

This thesis is part of a Tekes-funded project, whose objective was to develop a Ready-to-use microfluidic cartridge for affordable Point-of-Care Diagnostics (shortly ReDia). The testing cartridge would detect tuberculosis and cardiac troponin I (cTnI) markers. The project was performed in cooperation with Tampere University of Technology (TUT), University of Turku (UTU/DBUT) and University of Delhi (UDSC). Companies involved in the project were DHR Finland/Innotrac Diagnostic, Jatec, Kaivogen, Kaptas, Medisize, Medix Biochemical, NanoFoot and Span diagnostics Ltd. (India). The department of Automation Science and Engineering (ASE) in TUT acted as the project coordinator and was responsible for microfluidics. The department of Production Engineering (TTE) in TUT focused on assembling the cartridges and provided knowledge on laser welding. The department of Biotechnology in UTU provided insight about nanoparticles and other chemistry needed in the cartridge. The project was organized into three work packages.

The first work package contained all production technologies needed for the cartridge manufacturing. Channel fabrication and bonding studies were included here, as well as, gamma irradiation treatments and reagent deposition studies.

The second work package focused on the study of a microfluidic tuberculosis assay. The main objective was to develop a direct immunoassay test, which used the M. Tuberculosis antibodies, in order to detect the respective antigens. The test was intended to be simple and cheap yet still sensitive enough to fill the gap in tuberculosis diagnostics.

The third work package focused on the development of various methods for a cardiac Troponin I assay (cTnI). Here, the reaction chamber for a heterogeneous cTnI assay was designed and experimentally tested by Jari Väliaho. Another major task of this work package was the development of microfluidic sample pre-processing methods, which was split into two parts: increasing the robustness of the volume metering area, done by Rokon Udin, and investigating the mixing efficiency, which is covered in this thesis.

1.2 Overview of thesis

The main goal of this thesis was to study the efficiency of various microfluidic mixers. By taking into account manufacturing procedures and costs, several mixer geometries were designed and tested. The mixing efficiency was studied by using a finite element method (FEM) approach. The purpose of the modeling was to provide a better understanding of the flow behavior in the cartridge, as well as, a quantitative assessment of the efficiency for each mixer type.

The structure of the thesis is as follows: Chapter 2 provides some theoretical background on Point-of-Care (POC) devices and microfluidic concepts. In addition, a more in depth overview of microfluidic mixers and the basic principle of FEM modelling is also presented. Moreover, a short literature review of the evaluation methods for the mixing efficiency used in both the simulations and the measurements is presented. Chapter 3 describes the developed models, as well as the materials and methods used for simulation and concept verification. Chapter 4 presents and discusses the results of the study and chapter 5 concludes the thesis.

2. THEORETICAL BACKGROUND

This chapter covers the theoretical concepts necessary for understanding the thesis. In the first section, POC diagnostics concepts are introduced. The key microfluidics concepts are shortly described in the second section. The third section focuses on mixing within microfluidic channels, and presents different micromixer types. The fourth section provides an overview of the methods used to evaluate the mixing efficiency of micromixer. The last section explains the basic concepts regarding FEM-based modelling.

2.1 Point Of Care Diagnostics

2.1.1 In-vitro Diagnostics

In-vitro diagnostics (IVD) refers to any testing method that is performed outside of a living body, in an artificial environment. The purpose of these methods is not to provide a direct therapeutic effect, but rather to characterize a particular condition. Typically, IVDs are used in characterizing, monitoring and controlling a disease progression, such as diabetes or respiratory disorders. Moreover, they can be used to detect new strands of potentially serious epidemic agents (i.e. various bacterial or viral infections). In addition, they can be used in synthesizing a cure for these agents. [1] Based on the location where the tests are performed, IVD tests can be split into three main categories: Clinical, Near-patient and Self-testing.

Clinical IVDs contain all tests that are generally too complex and need to be run by a specialist, under laboratory conditions. The sample is sent to the laboratory, and after analysis, the results are reported back to the person requesting the test.

Near-Patient tests refer to any type of test that can be carried out by a professional, outside a specialist laboratory conditions. The results are generally obtained quite fast and are typically used to provide a preliminary diagnosis of a condition.

Self-Testing refer to any IVD method that is designed to be used by an individual. They usually do not require any training for carrying and interpreting the tests. Examples include blood sugar tests, pregnancy test, etc. This particular type has seen an increase in recent years, since the devices have become easier to use and provide more accurate results. [1]

IVDs play a critical role in determining a patient's healthcare needs. They offer a preliminary diagnosis that in many case can help the patient. Moreover, IVD devices provide users an early diagnosis, which can prevent long term effects. [1] Generally, the devices

used in IVD tests are minimally invasive, thus preventing most of the complications that would arise in *in vivo* tests.

2.1.2 Point Of Care Testing

Point of Care testing (POCT) refers to any IVD that is performed in close proximity to the patient receiving care. Generally, POCT is performed by non-laboratory personnel and are used for clinical purposes. They are typically more expensive than the clinical laboratory tests, but since the test are performed near the patient, it allows immediate decision making for the personnel. [2]

Based on the type of diagnosis it provides, the global POC diagnostic market is categorized into: infectious disease, glucose monitoring, coagulation monitoring, urinalysis testing, hematology, cholesterol, abuse of drugs, cardiac markers, blood gas/electrolytes, tumor/cancer makers, pregnancy and fertility tests, food pathogens tests and others. Based on the end user and prescription modes, POCT can be classified into: Near-patient and Self-monitoring kits. [3]

Currently, the largest market share belongs to the glucose monitoring kits, which occupy almost half of the market. The cardiac marker -, infectious disease testing -, coagulation monitoring - and the pregnancy and fertility testing kits occupy a large portion of the remaining market. For 2018, [3] forecasts a similar increase in the revenues for all POCT sectors. The market is dominated by various players, such as, Roche Diagnostics Ltd. (CH), Siemens AG (DE), Alere Inc., (US), Johnson & Johnson (US), Bayer AG (DE), etc. [3]

2.1.3 Lab-On-a-Chip

As the name suggests, the Lab-On-a-Chip (LOC) devices are POC diagnostic devices which allow for IVD tests to be run with smaller fluid volumes. By using microfluidic concepts, LOCs have the potential to miniaturize complex laboratory procedures on a small microchip. They have several advantages over conventional methods, such as: small volumes of samples and reagent and fast result generation. New LOC methods will emerge by either adapting LOC components into an existing non-LOC POC technology, or re-working current concepts into a practical devices, such as the M. Tuberculosis or cTnI microfluidic cartridges from the ReDia project. Based on the type of analyte they study, current LOCs can be divided into four major categories. [4]

Small molecules. A classic example of these type of LOCs is the iSTAT device, which was a novel microsensor, developed by micro fabricating thin-film electrodes on silicon chips. These chips are used to detect various blood chemistries (sodium, potassium, chloride, glucose, gases, etc.), coagulation and cardiac markers. The iSTAT devices is a

handheld battery-powered analyzer, which targeted primarily for emergency and critical care conditions. [4]

Cells. These type of LOCs are currently mostly used for monitoring HIV/AIDS by counting the presence of CD4 T-cells. Some of the devices belonging to this category are currently either in Food and Drug Administration (FDA) approval stages or have already been approved. [5]

Nucleic acids LOCs are used for the detection of DNA and RNA signatures for diagnostic purposes, as well as monitoring patients at the point of care. Generally, there is an increase in the number of companies that develop nucleic acid-based assays, due to the increase in the clinical demand for nucleic acid detection. [4]

Immunoassay based LOCs typically use a disposable cartridge, in which the fluorescence signal, or any other signal, is detected. This technology uses labeled particles that bind to the immunoassay, in order to detect the presence of a particular compound. One big drawback of this type is that the devices do not yet work with finger-pricked whole blood samples, but still require centrifugation of blood samples. [4]

2.2 Microfluidic Principles

All of the LOC devices use the concept of microfluidics in their functioning. Since they use small fluid volumes, capillary effects and other related microfluidic concepts will be discussed briefly in this section.

2.2.1 Fluid and Scaling Effect

There are four states of matter: solid, liquid, gas and plasma. In the solid state the particles are closely packed together through molecular interactions and are packed in a regularly repeating ordered structure, also known as lattice. Due to these interaction forces the particles cannot freely move, but can only vibrate. As a result a solid has a definite shape and definite volume. Fluids include both liquids and gasses, and do not have such a strict configuration. Microfluidics, as defined by [6], “deals with the flow of fluids and of suspensions in sub millimeter-sized systems”.

Fluid mechanics studies are conducted under the assumption that the fluid of interest can be treated as a continuum. This is known as the continuum assumption or hypothesis. This means that all quantities of interest, such as density, velocity or pressure can be defined at any point in space and vary continuously from point to point in the flow. Microfluidics deals with structures that are in the order of tens of micrometers or larger. In this range there are enough molecules contained in the fluid for the continuum assumption to hold. However, in the nanometer range, the number of particles is not sufficient for the

hypothesis to hold. Here, molecular approaches to conventional fluid mechanics must be used to accurately characterize the fluid and its flow. [6, 7]

2.2.2 Single-Phase Flow

In the most general point of view, fluid flow is determined by the knowledge of velocity (v), pressure (p), density (ρ), viscosity (η), specific heat (C_p) and temperature (T). For any fluid density, viscosity and specific heat are related to pressure and temperature by equations of state (EOS). Thus, we are left with five unknowns: v_x, v_y, v_z, p and T. They are related by a system of three equations: a scalar equation for conservation of mass, a vector equation for conservation of momentum and a scalar equation for conservation of energy. This system of equations is often referred to as the Navier-Stokes (NS) equations. [8] The first equation is the *conservation of Mass* or *Continuity* equation.

Let the velocity field be given by (v_x, v_y, v_z) and (x, y, z) the Cartesian coordinate system. The equation may be written, in vector form, as:

$$d_t \rho + \rho \nabla \cdot v = 0 . \tag{1}$$

where,

$$d_t = \frac{\partial}{\partial t} + v_x \frac{\partial}{\partial x} + v_y \frac{\partial}{\partial y} + v_z \frac{\partial}{\partial z}, \text{ and } \nabla = \frac{\partial}{\partial x} + \frac{\partial}{\partial y} + \frac{\partial}{\partial z} .$$

In the case of incompressible fluids, Equation (1) reduces to:

$$\rho \nabla \cdot v = 0 . \tag{2}$$

The second equation is the *Momentum conservation* equation. [8] refers to this equation as the NS equation, rather than the whole system. It states that the change in momentum of a fluid is equal to the balance between inlet momentum, outlet momentum and exerted forces. In its vectorial notation the equation is:

$$\rho(\partial_t v + (v \cdot \nabla)v) = -\nabla p + \eta \nabla^2 v + \beta \eta \nabla(\nabla \cdot v) + \rho g + \rho_{el} E \tag{3}$$

where β is a dimensionless viscosity ratio, ρ_{el} is the charge density, g is the gravitational force vector and E the electrical force vector.

For incompressible fluids, Equation (3) reduces to:

$$\rho(\partial_t v + (v \cdot \nabla)v) = -\nabla p + \eta \nabla^2 v + \rho g + \rho_{el} E . \tag{4}$$

The *Energy conservation* equation is, in Cartesian coordinates,

$$\rho C_p\left(\frac{\partial T}{\partial t}+v_x\frac{\partial T}{\partial x}+v_y\frac{\partial T}{\partial y}+v_z\frac{\partial T}{\partial z}\right)=\frac{\partial}{\partial x}\left(k\frac{\partial T}{\partial x}\right)+\frac{\partial}{\partial y}\left(k\frac{\partial T}{\partial y}\right)+\frac{\partial}{\partial z}\left(\frac{\partial T}{\partial z}\right)+q, \qquad (5)$$

where k is the conduction coefficient and q is the source or sink term.

The Navier-Stokes equation has analytical solutions for several classes of flows. Of particular interest is the pressure-driven, steady state flow in channel, known as Hagen-Poiseuille flow. This class is of major importance for the basic understanding of any liquid handling in LOC systems. In this type, fluid flow is generated by imposing a pressure difference between the two ends of a rigid channel. [6]

Since the cross-section shape of the channel varies from application to application, an arbitrary cross-section is generally considered for defining the structural form of the velocity field. [6]

The channel is parallel to the *x*-axis and it is assumed to be invariant in that direction, seen in Figure 2-1. Let C be an arbitrarily shaped cross-section of the channel in *yz*-plane and ∂C –boundary in *yz* direction. The pressure difference (Δp) over a segment of length (L) is assumed to be constant.

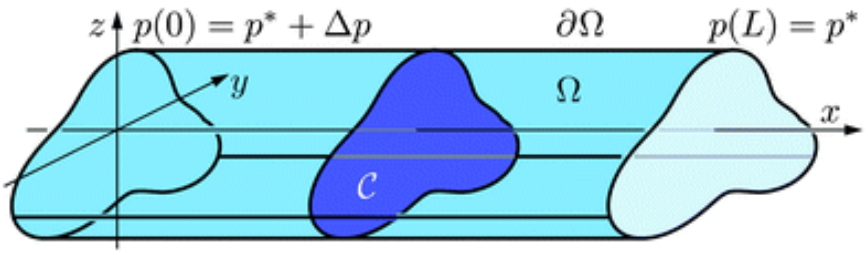

Figure 2-1. *Poiseuille-flow problem in an arbitrary cross-section channel, which is transitionally invariant to x-axis. Image taken from* ***[6]***

For Poiseuille flows there is a translational invariance of the channel in the *x*-axis, as well as, vanishing forces in the *xy*-plane. This implies that the velocity field does not depend on *x*-axis. Moreover, only the *x*-axis component of the velocity field is non-zero. This means that the partial derivatives of the pressure fields with respect to the *y*- and *z*-axis are zero, signifying that the pressure field only depends on the *x* component. The *x*-axis component of the Navier-Stokes equation, under the abovementioned conditions becomes:

$$\eta(\partial_y^2+\partial_z^2)v_x(y,z)=\partial_x p(x) \qquad (6)$$

The assumption that the pressure gradient ($\partial_x(p(x))$) is constant, implies that the pressure must be a linear function of *x*. The final partial differential equation for $v_x(y,z)$ at the boundary *C* and the solid walls described by ∂C is given below.

$$\begin{cases} [\partial_y^2 + \partial_z^2] v_x(y,z) = -\dfrac{\Delta p}{\eta L}, \ \forall\ (y,z) \in C \\ v_x(y,z) = 0 \qquad\qquad\qquad \forall\ (y,z) \in \partial C. \end{cases} \tag{7}$$

After determining the velocity field, one can compute the volumetric flow rate (*Q*) and the mass flow rate (Q_{mass}), by using equations (8) and (9) respectively. The volumetric flow rate is defined as the fluid volume discharged by the channel per unit time, while the mass flow rate as the discharged mass per unit time.

$$Q \equiv \int_C v_x(y,z)\,dydz \tag{8}$$

$$Q_{mass} = \int_C \rho v_x(y,z)\,dydz \tag{9}$$

Figure 2-2 shows the flow profile of a Poiseuille flow for an infinite, parallel-plate channel of height *h*. It can be used to approximate the expression for the flow rate and flow speed, for a flat rectangular channel. [6] The pressure drop (Δp) is evaluated over a section of length (*L*).

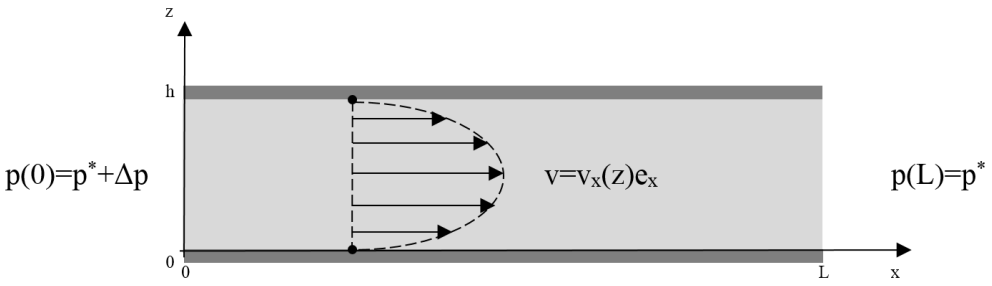

Figure 2-2. *Sketch of xz-plane of an infinite parallel-plate channel of height h. Figure adapted from* ***[6]****.*

The flow rate through a section of width *w*, becomes:

$$Q = \int_0^w dy \int_0^h dz\, \frac{\Delta p}{2\eta L}(h-z)z = \frac{h^3 w}{12\eta L}\Delta p\,. \tag{10}$$

Equation (10) is an approximate expression of the flow rate in a rectangular cross section channel. For our studies a more useful flow solution would be for channels with a circular cross-section, with a radius $a=h$ and $a=w$. Equations (11) and (12) describe the velocity and flow rate in the case of a circular cross-section channel. [6]

$$v_x(y,z) = \frac{\Delta p}{4\eta L}(a^2 - y^2 - z^2) \tag{11}$$

$$Q = \frac{\pi a^4}{8\eta L}\Delta p \tag{12}$$

where: a is the radius of the circle, η is the dynamic viscosity of the fluid, L is the length of the considered channel. [6]

Lumped element modelling is a modeling tool, through which we can correlate mechanical, biological or chemical quantities with electric circuit quantities. Generally, this modelling tool is employed when studying complex systems, in which we have both electrical and non-electrical elements, but can also be used for microfluidics.

Conjugate power variables are quantities whose product yields the net power flow between two elements. For an electrical circuit, the conjugate variables are the voltage difference, ΔV, and the current, I, whose product yields the electric power, P. For incompressible flows, the conjugate power variables are the pressure difference, Δp, and the flow rate, Q. We can define the equivalent resistance of a microfluidic system, known as the *hydraulic resistance*, by making the analogy to the electrical resistance of an electric system, R, and Ohm's law ($\Delta V = RI$). This leads to Equation (12). [9]

$$R_{hyd} = \frac{\Delta p}{Q} \tag{13}$$

2.2.3 Laminar Flow

There are generally three types of flow regimes for a fluid: laminar, transient and turbulent. A way to determine the flow regime of a particular fluid is the Reynolds number, which is defined in Equation (14). It characterizes the importance of the inertial forces to the viscous ones. [6]

$$\mathrm{Re} = \frac{\rho v D_h}{\eta} \tag{14}$$

where D_h is the hydraulic diameter.

A laminar flow regime corresponds to a Reynolds number smaller than 2000. In a laminar flow the fluid travels smoothly or in regular paths. The flow properties, such as velocity or pressure, do not vary with time. [8]

$$D_h = 4\frac{A}{P} \tag{15}$$

The hydraulic diameter (Equation (15)) is defined as the as the ratio between the cross section area (A) of the channel and the wetter perimeter (P). [8]

2.2.4 Capillary Effects

A key characteristic of microfluidics is the dominance of surface effects. This is due micro fluids having a higher surface to bulk ratio. The most important class of surface effects is known as the capillary effect. Capillary effects can be understood by studying Gibbs free energy (G). It is the energy of systems where the thermodynamic control parameters are pressure (p), temperature (T) and particle number (N). In particular, the equilibrium situations are used, where the Gibbs free energy is, by definition, minimum. [6]

Surface tension is a main concept in surface science and generally depends on the two materials on each side of the surface. The surface tension, γ, for an interface is defined as the Gibbs free energy per unit area at fixed temperature and pressure, see Eq. (16). [6]

$$\gamma \equiv \left(\frac{\partial G}{\partial A}\right)_{p,T} \tag{16}$$

Another key concept in surface theory is contact angle, θ. It is defined as the angle between the interfaces where three immiscible phases meet (liquid, gas, solid). In the equilibrium case, θ is determined by Young's equation, which relates the surface tensions between the interfaces, as seen in Eq. (17). [10]

$$\cos\theta = \frac{\gamma_{sg} - \gamma_{sl}}{\gamma_{\mathrm{lg}}} \tag{17}$$

where γ_{sg} is the surface tension between the solid and gas phases, γ_{sl} is the surface tension between the solid and the liquid phases and γ_{lg} is the surface tension between the liquid and gas phases.

There are generally two types of contact angles. The first type of contact angle is the *static contact angle* and it is measured by placing a single droplet on a surface. Once thermodynamic equilibrium, between the three phases, is reached the contact angle is measured, see Figure 2-3.a). The second type of contact angle is the *dynamic contact angle* and the most common methods for measuring it is the tilting plate method. After a droplet is placed on a solid surface, the surface is inclined at an angle t, typically from 0° to 90°. The droplet will start to roll off the solid at a certain angle, called roll-off angle, once wetting occurs. At this angle the advancing (θ_a) and receding (θ_r) droplet contact angle are then measured, see Figure 2-3.b) [10]

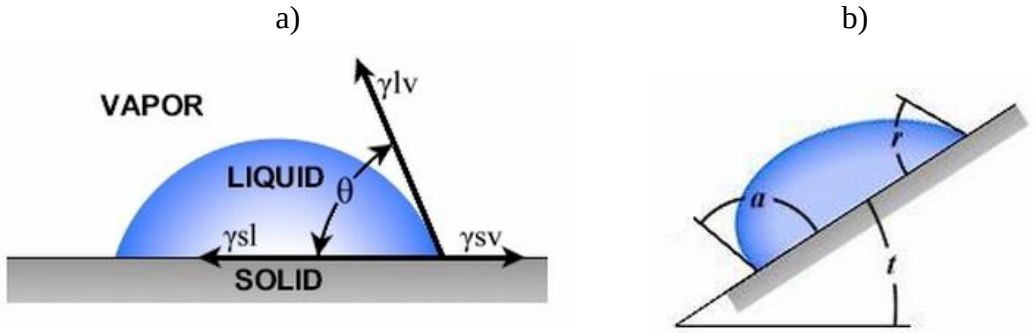

Figure 2-3. *(a) Static contact angle θ is measured as the angle between the interfaces according to Equation (17). (b) Dynamic contact angle measurement example, using tilted plate method. Here the advancing and receding contact angles are measured individually. Images taken from* ***[10]****.*

By measuring the contact angle of an aqueous liquid on a surface, one can determine whether the surface is hydrophobic or hydrophilic. Hydrophobic surfaces will have a contact angle larger than 90° and non-wettable, while hydrophilic surfaces will have a contact angle smaller than 90° and wettable. [6]

2.2.5 Plug Flows

Generally, it is quite common to have two immiscible fluids that flow through a microchannel. As an example one can have a gas and liquid phase flowing inside the channel, shown in Figure 2-4, where A-F are points between which the pressure drops are measured. These pressure drop can be either due to friction (i.e. A-B) or due to capillary forces (i.e. B-C).

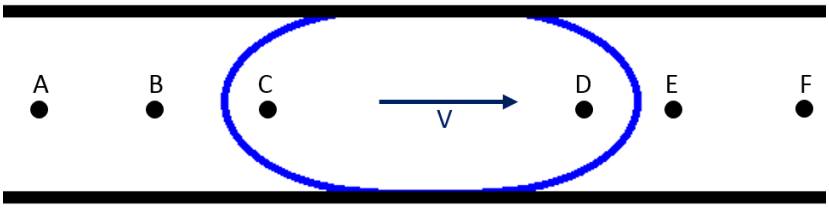

Figure 2-4. *Lumped element decomposition of a two phase flow. Between points A - B, C - D and E - F there are only pressure drops due to friction. Between points B - C and D - E there are pressure losses only due to capillary forces. Figure taken from* ***[8]****.*

For moving the liquid plug inside the channel pressure can be used. Additional to the friction losses, taken into consideration in single phase flow analysis, there are capillary forces that introduce pressure losses. These capillary forces affect both ends of the liquid plug. Thus, the overall pressure losses inside the channel are given by:

$$\Delta p_{chanel} = \Delta p_{friction} + \Delta p_{capilary} \tag{18}$$

with the two components defined as:

$$\Delta p_{friction} = \frac{8\nu}{a^2}(\eta_1 L_1 + \eta_2 L_2), \tag{19}$$

$$\Delta p_{capillary} = \frac{2\gamma}{a}(-\cos\theta_a + \cos\theta_r), \tag{20}$$

where, a is the radius of channel cross-section (circular cross-section channel), η_i is the dynamic viscosity of liquid i, γ is the surface tension between the two phases, θ_a the advancing contact angle and θ_r is the receding contact angle.

2.2.6 Diffusion

Given a solution consisting of a solute (i.e. particles) and a solvent (i.e. liquid, in which particles are dissolved in), diffusion is defined as the motion of the solute in the solvent from regions of high concentration to regions of low concentration. Pure diffusion of the solute occurs when the velocity field of the solvent is zero. When the solvent velocity field is different from zero, the motion of the solute is partially convective. [6]

A way to model diffusion is to analyze Equations (1) and (3) in the case where there are several fluids mixed. In equations (1) and (3) the fluid had a homogeneous density (ρ). Let α be the number of fluids in the solution and ρ_α the density of α fluid. The total fluid density is given by the sum of all fluid densities:

$$\rho \equiv \sum_\alpha \rho_\alpha \tag{21}$$

Let $C_\alpha(t) = \frac{\rho_\alpha(t)}{\rho(t)}$ be the dimensionless concentration of solute α at time t. By using the mass current density equation and Fick's law for diffusion current density, for solute α we obtain the general convection-diffusion equation for a solute α, having a velocity field v,

$$\underbrace{\frac{\partial C_\alpha}{\partial t}}_{\substack{mass\ current \\ density}} + \underbrace{v\nabla C_\alpha}_{\substack{convection\ current \\ density}} = \underbrace{D_\alpha \nabla^2 C_\alpha}_{\substack{diffusion\ current \\ density}}, \tag{22}$$

where D_α is the diffusion constant or coefficient for solute α.

From equation (22) the diffusion equation is derived. Since in pure diffusion the velocity field is zero, the convection term is absent. The coefficient c_α is the concentration given by the number of molecules of per volume. It is related to C_α, from Equation 22, by multiplying it with the total density (ρ) and dividing it with the mass (m). If we consider the

diffusion of only one solute. the index α is suppressed. Moreover, for pure diffusion, the velocity field is zero, which leads to the diffusion equation shown below. [6]

$$\frac{\partial c}{\partial t} = D\nabla^2 c. \tag{23}$$

The average diffusion time τ_{diff} over a mixing length d is given by [6]:

$$\tau_{diff} = \frac{d^2}{2D} \tag{24}$$

The average convection time τ_{conv} is for a flow velocity v and channel length L given by:

$$\tau_{conv} = \frac{L}{v} \tag{25}$$

2.3 Micromixers

Rapid mixing is essential in many microfluidic systems used in areas, such as: biochemical analysis, drug delivery devices and sequencing or synthesis of nucleic acids. Most biological processes or enzyme activation processes require mixing of reactants for reaction initiation. In LOC applications mixing is necessary to promote complex chemical reactions. [11] In all of the cases mentioned above, there are two or more solutions that need to be mixed together. While in macroscale this is achieved through turbulence, in microscale the mixing relies mostly on diffusion, detailed in Section 2.2.6, due to the laminar flow behavior of the fluid. [7]

Micromixers, thus are an important component of most microfluidic systems. They are generally classified based on the need for external energy to achieve mixing. Thus, we distinguish between two classes of micromixers: passive and active. Passive micromixers rely solely on the fluid pumping energy (i.e. pressure) to achieve mixing. Active micromixers, on the other hand, rely on additional external energy as well as the pumping energy. [7, 10-12]

When designing a micromixer there are some additional quantities that need to be taken into consideration. The previously defined Reynolds number, Diffusion coefficient and Diffusion time are important in micromixers. Additionally, the Peclet (Pe) and Strohal (St) numbers are used. The Peclet number (Equation (26)) relates the mass transport due to convection to the mass transport due to diffusion. The Strohal number (Equation (27)) is the ratio between the residence time of a species and the time period of its disturbance. [11] The Strohal number is important in characterizing active micromixers.

$$Pe = \frac{vL}{D}, \tag{26}$$

$$St = \frac{fD_h}{v}, \tag{27}$$

where f is the disturbance frequency.

2.3.1 Passive Micromixers

Because passive mixers rely solely on the fluid pumping energy for mixing, they are still the most common type of mixer used in most microfluidic applications, since they are easier and cheaper to be manufactured, have less active parts and are more robust. [12] Due to the laminar flow in the channels, the mixing is achieved by diffusion and chaotic advection. There are three major types of passive micromixers based on the arrangement of the mixing phases: lamination, chaotic advection and droplet micromixers.

Lamination mixers

The lamination mixers can be further split into two main categories: serial and parallel [11, 13]. The most basic type of passive lamination mixers consists of a long microchannel with two inlets. Based on the junction shape, they are called T-mixers or Y-mixers and are shown in the Figure below. As standalone micromixers, T- and Y-mixers are one of the most heavily studied and used type, due to their simplicity and robustness. Furthermore, when studying more complex micromixer geometries, they are used as inlets for the two streams. [14, 15, 16]

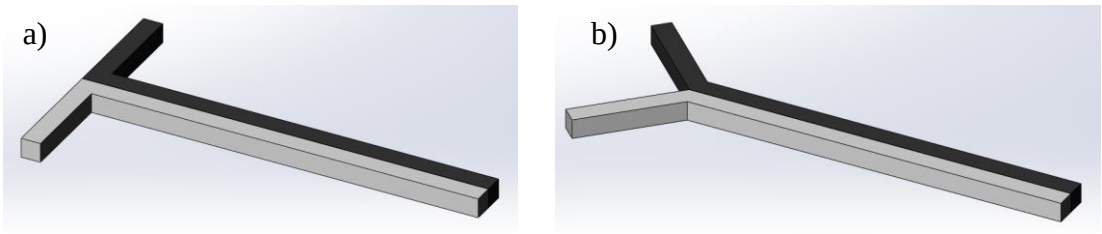

Figure 2-5. *(a) T-mixer and (b) Y-mixer.*

Generally, faster mixing can be obtained by decreasing the mixing path, while increasing the contact surface between the two phases. In parallel lamination the inlet stream is split into *n*-substreams and then joined back into one stream, as laminae. Parallel lamination involves separating the two phases into liquid "sheets" to reduce the mixing path. [11] Most T- and Y-mixers require a long channel in order to achieve a satisfactory mixing of the two streams. This is seen as a drawback, since in almost all applications there will be a space limitation. In contrast, a subdivision of each stream into *n*-laminae decreased the mixing time by a factor of n^2. An example of a parallel micromixer is shown in Figure 2-6 a). [13] A classic example of parallel micromixers is the hydraulic focusing type,

Figure 2-6 b), which uses three inlets. The middle inlet, containing a sample solution, is focused between the two side inlets, containing solvents. This produces a narrow stream of the focused solution, which decreases the mixing time considerably.

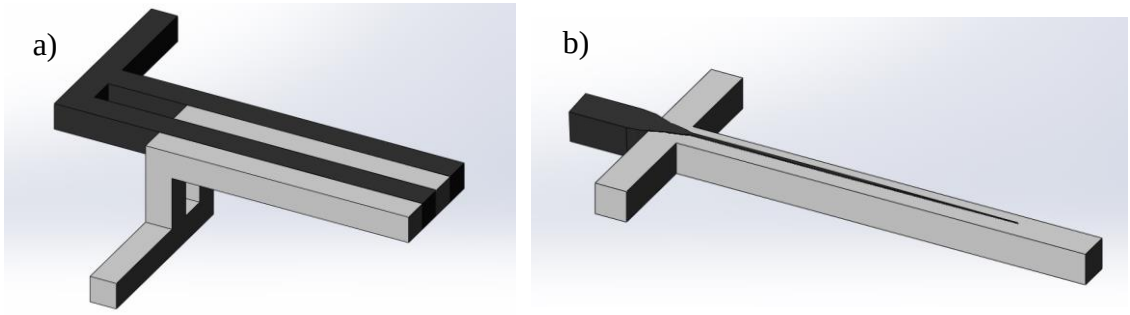

Figure 2-6. *(a) Example of a parallel lamination micromixer; (b) example of a hydraulic focusing micromixer; concepts adapted from* ***[11]****.*

A similar approach to parallel micromixers is used in the serial lamination micromixers. They are known also as sequential or split-and-recombine mixers. The difference between the parallel and the serial types lies in the method used to achieve the lamination of the fluids. In serial mixers, the lamination is obtained via a sequential process, which generally has three major stages: flow splitting, flow recombining, and flow rearrangement. [13] After *m* splitting and joining stages, there will be 2^m liquid layers, which in turn improves the mixing time by a factor of 4^{m-1}. [17] Examples of serial lamination micromixers are shown in Figure 2-7 [11]

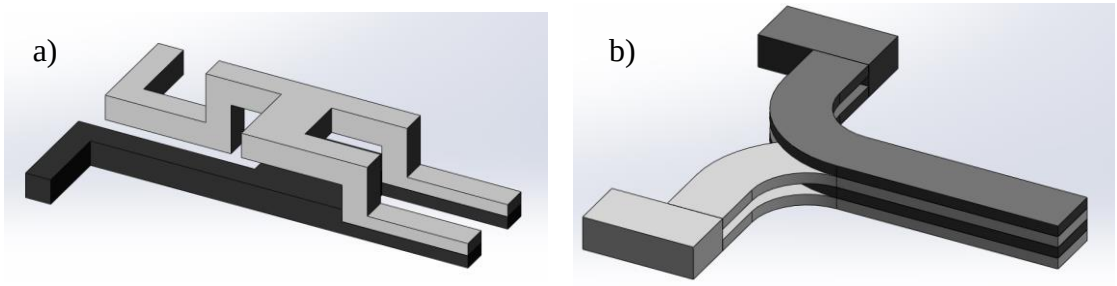

Figure 2-7 *Examples of a Split-and-Recombine lamination micromixers; concepts adapted from* ***[11]*** *and* ***[18]****.*

Chaotic advection

Aside from diffusion two fluids can mix via advection. Generally, advection is parallel to the main flow direction and is not useful for transverse flow mixing processes. This can be overcome by using the so called, chaotic advection. Special geometry modifications are used in order to increase the mixing in the transverse components. This is obtained by splitting, stretching, folding or breaking the flow. For microflows, there is a distinction between mixer types based on the Re number ranges. Often, there are three ranges used: high Re number (>100), medium Re number (10-100) and low Re number (<10). [11]

The simplest method of obtaining chaotic advection mixing is to introduce obstacles, either in the flow path or on the channel walls, shown in Figure 2-8. These geometries induce flow eddies and recirculation, and are used for high Re number mixers. In addition to obstacles, zig-zag or serpentine channel shapes can be used to improve the mixing efficiency. [11]

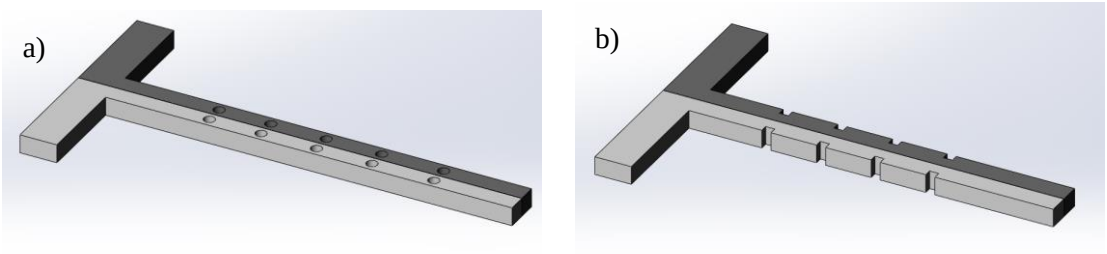

Figure 2-8. *Chaotic advection micromixer examples: (a) obstacles in the flow path; (b) obstacles on the channel walls; concepts adapted from* ***[11]****.*

At medium Re numbers, the micromixer designs were derived from their macroscopic counterparts. For example, there were 3-dimensional twisted structures, derived from twisted conducts and 3-dimensional serpentine geometries reported. Moreover, a modified Tesla structure was used to generate Coanda effects in the flow. These geometries are generally difficult and expensive to manufacture.

At low Re numbers rips or grooves on the channel walls can be used to induce chaotic advection mixing. Similar to the high Re numbers, the geometries produce eddies and recirculation of the flow. Some important structures are shown in Figure 2-9. [11]

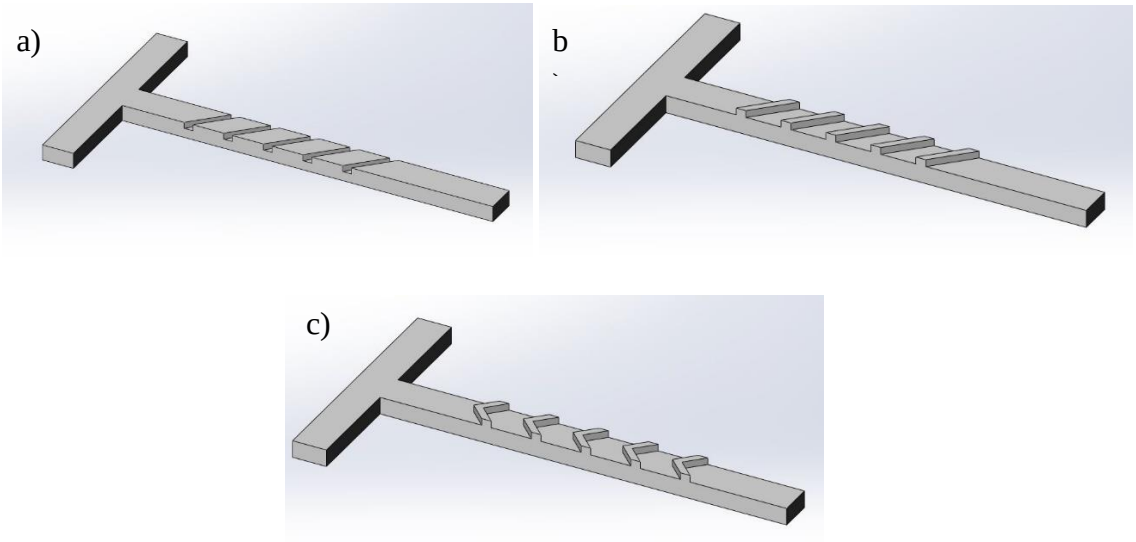

Figure 2-9. *Chaotic advection micromixer examples: (a) channel rips; (b) channel grooves; (c) staggered-herring bone; concepts adapted from* ***[11]****.*

Droplet micromixers

A completely different approach for decreasing the mixing path is to form droplets of the mixing liquids. The movement of the droplet generates an internal flow field, allowing for the mixing of the liquids inside. The transport of the droplets can be achieved using pressure or capillary effects (i.e. thermocapillary, electrowetting). A simple design of droplet micromixers would include: a carrier fluid (i.e. oil, air) in which droplets are formed (i.e. mixture of buffer and sample solution). A critical requirement for this is that the carrier fluid and the droplet mixture to be immiscible. Mixing within the droplet is accelerated by the sheer forces with the carrier fluid. [11, 13]

2.3.2 Active Micromixers

Active micromixers rely on an external energy source, as well as the fluid pumping energy to accelerate the mixing process. This is achieved by introducing time-dependent perturbations in the channel that stir and perturb the flow. There are eight classes of active micromixers, based on the external energy used. In all cases the active mixer has a higher mixing efficiency, however they require the integration of peripheral devices (i.e. actuators). The micromixers are more complex, more expensive to fabricate and are generally not suitable for biological applications, as the components might damage the samples. [13]

Pressure Field Disturbance micromixers enhance mixing by producing pressure field disturbances in the flow path, such as: flow segmentation (by using alternative starting/stopping miropumps, or periodically oscillating flow rates), flow discretization (vortex miropumps). Furthermore, microstirrers are integrated in the channel, which are controlled by external magnetic field. [11, 12]

Electro-hydrodynamic active micromixers use electrodes, placed along the mixing path, to increase the mixing performance, which is achieved by changing the voltage and the frequency of the electrodes. [11, 17]

Dielectrophoretic micromixers use the polarization of a particle, relative to its surrounding medium in an alternative electric field, allowing the particle to move to and from an electrode. The micromixers use embedded particles in the liquids to be mixed, together with two electrodes. By changing the electric field polarity, the particles mix the liquids. [11]

Electrokinetic micromixers use a fluctuating electric field to introduce mixing in the microfluidic channel. This field causes rapid stretching and folding of the fluid interfaces, allowing for the two fluids to stir. The fluctuating electric field can be induced by using an alternating current voltage source. [13]

Magneto-Hydrodynamic mixers rely on inducing Lorentz forces in an electrolyte solution. The mixer uses an array of electrodes placed on the channel walls that, in the presence of an alternate potential difference on the electrodes, induce current flows within the fluids to be mixed. By coupling the generated electric field with a magnetic field one can generate the Lorentz body forces. [13]

Acoustic micromixers use acoustic stirring, which is created by ultrasonic waves. The waves are induced, generally by using acoustic actuators (i.e. piezoelectric ceramic transducers) integrated in the channel. They cause stirring of the fluid perpendicular to the flow direction, leading to enhanced mixing within the channel. [13]

Thermal disturbance mixers rely on the fact that the diffusion coefficient depends heavily on temperature. By increasing the fluid temperatures the mixing times decrease heavily. [11]

2.4 Mixing Efficiency Evaluation Techniques

Evaluation from Finite Element Methods

The most common approach for evaluating the mixing efficiency of micromixers is to first simulate the flow behavior using FEM software and then to confirm the results by experimental validation. [16], [15]. The flow profile is similar to that obtained from Particle Image velocimetry (PIV) measurements. Generally, this approach is used in lamination micromixers, since the flow profile is easy to predict. From the chaotic micromixers, presented in Section 2.3.1, the most studied micromixer is the staggered herringbone micromixer, where the herringbone elements are extruded from the channel surface, presented in Figure 2-9 c). The most common evaluation methods include particle tracking ([19]), relative variance of the concentration profile ([20] and [21]) and flow helicity ([22]).

In [19], the velocity profile was used to estimate the particle trajectories. At a given cut plane, the coefficient of variance of the particle distribution was computed, computed as the standard deviation of the particle distribution divided by the mean. The cut planes in this study were positioned after a set of staggered herringbone elements. For homogeneous mixing the coefficient of variance should be zero. The mixing performance of the micromixer was evaluated at five Re numbers.

Du, et al., [21], used the concentration profiles to compare the staggered herringbone micromixer with the slanted groove micromixer. The concentration was evaluated at different channel lengths for particular channel width and height combinations. Moreover, the groove height was varied for both structures, and the concentration profile was evaluated at different, fixed cross-section locations. The results showed that increasing the element height above a certain threshold no longer improved the mixing efficiency.

In [20], the optimization of the slanted herringbone micromixer consisted of two sequences: First, the herringbone geometry was optimized, based on the velocity magnitude at the end of a groove element, and then different configurations of six herringbone grooves were studied. The evaluation of the mixing efficiency was done by computing the concentration variance at a particular cut plane, defined as:

$$S = \frac{\left(\int_{Ax} (c_x - c_\infty) dA_x \right) \Big/ A_x}{\left(\int_{Ain} (c_{inlet} - c_\infty) dA_{in} \right) \Big/ A_{inlet}} \tag{28}$$

Where x represent the x-plane position of the cut plane and c_∞ represents the concentration variance when the two fluid are perfectly mixed (when $x \to \infty$)

Evaluation from Experimental Testing

Any FEM model needs to be experimentally validated. For micromixers, this is most commonly done by mixing two optically different, miscible fluids in the channel. In [23] a mixture of gold nanoparticles solution (20 nm) and CuSO4 (100 mM) was used. [24] used water and ethanol, while [25] used a glycerol-water solution with a colored food dye. In all three cases, a charged coupled device (CCD) was used to image the fluid mixing. Here, the experimental validation of the models offered a more of a qualitative assessment of the mixing, suggesting that it is enough to prove that the mixers behave in a manner, similar to the simulated models.

In [15] a mixture of NaAc/KI/KIO3 and HCl were used to evaluate the mixing, by using ultraviolet (UV) characterization. The UV absorption analysis revealed that inefficient mixing causes an increase in iodine concentration in the NaAc/KI/KIO3 mixture.

Confocal microscopy was used in [14] to quantify the mixing efficiency of a staggered herringbone micromixer, by taking micrographs of vertical cross-sections. A water/glycerol solution, with water containing a fluorescent solution, was injected into the channel. The standard deviation of the fluorescence intensity was used to characterize the herringbone element dimensions. The study revealed that a particular width ratio (see Section 3.3) yields the most efficient mixing for this type of micromixer.

Another experimental validation technique is the PIV method used by [26, 27]. This method measures the velocity components of particles flowing inside a channel. However, the results obtained from this method only verify the particle behavior inside the channel, rather than offer a quantitative assessment of the mixing. The behavior can also be verified using the techniques previously described.

2.5 Finite Element Method

The finite element method (FEM) is a numerical technique, which is used to approximate the solution of various partial differential equations (PDEs) that arise in applications. The purpose of this technique is to understand, predict and optimize the behavior of a studied system. The equations detailed in Section 2.2 are generally difficult to solve by using traditional methods (i.e. pen and paper) especially for complex geometries. [28]

In FEM modelling, the system is analyzed in a simplification or approximation of the real-life systems. Any geometry to be studied with FEM modelling, is a discrete version of the real system. Thus, the various PDEs are solved for discrete points, which are called nodes. Each node is only affected by its neighbors via the studied physics PDEs. Furthermore, the relationship of the system with its surroundings is described by the boundaries. [28, 29, 30]

The following example shows how the division of a geometry is done in FEM. For a rectangular microfluidic channel, see Figure 2-10, the geometry is divided into smaller elements (i.e. red triangle), which are connected to each other via nodes (black dots). The geometry contains 4 boundaries (blue, cyan, green, yellow) and is divided into 22 elements. Each boundary may have different properties, which are known as domain conditions. In this example, the green boundary would be the channel inlet, the cyan boundary the outlet, while the blue and yellow one would be the channel walls, which describe the relationship between the fluid and the wall itself. [30]

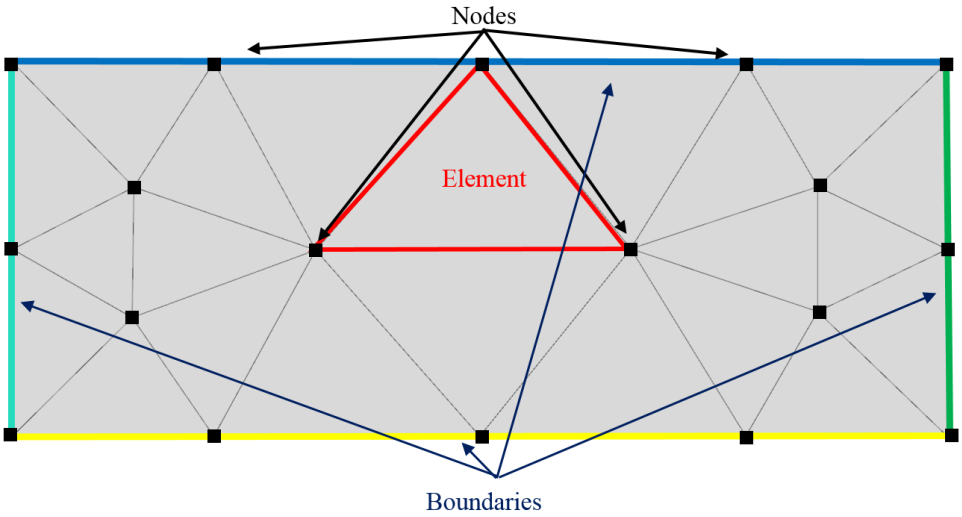

Figure 2-10. *Basic elements in a FEM model. This example has 4 boundaries (blue, cyan, green, yellow), 22 elements (red) and 18 nodes (black)*

Most FEM models follow the following basic steps. Firstly, a 2D or 3D geometry is created using Computer Aided Design (CAD) software. This geometry should closely approximate the studied system. Next, the domain and boundary conditions are defined, which depend on the studied physics. For example, the geometry presented in Figure 2-10

can be used to study fluid flow (fluidics) or beam bending under load (structural mechanics), in which case the boundaries have to be defined differently. In one case, the green boundary could be an inlet (fluidics), or could be the edge where the load is applied (structural mechanics). Afterwards, the geometry is meshed. Meshing is essentially the division of the geometry into smaller elements. Here one has to find a balance between the accuracy of the results and the simulation time, as both heavily depend on the number of nodes and elements. A too coarse mesh could result in the software not finding a solution, or having an extremely large error. A too dense mesh could result in the computer running out of memory or having too long computation times. Lastly the system is solved and the results are post-processed. [29, 30]

3. MATERIALS AND METHODS

3.1 Cartridge Overview

As the starting point, the ReDia project used a disposable immunoassay cartridge, which was designed in an earlier project, called NanoFlow, seen in Figure 3-1. The cartridge had the following components: sample channel (1), buffer channel (2), volume metering area (3), mixing area (4), dried Europium nanoparticle labels (5), reaction area containing a dried immunoassay surface (6), wash solution chamber (7) and a waste chamber (8).

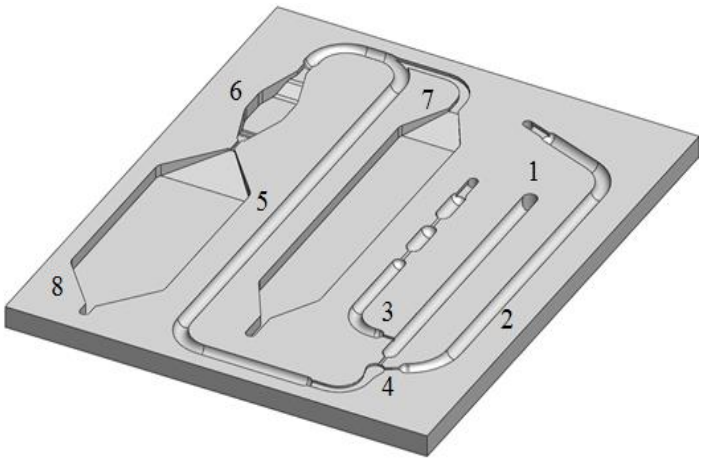

Figure 3-1. *Schematic of microfluidics immunoassay cartridges at the beginning of ReDia project*

The operation principle of the cartridge is as follows. First, the blood or plasma is inserted into the sample channel (1). Pressure is then used to drive the sample to the volume metering area (3). This volume metered sample is then combined with the buffer solution (2). The two compounds then pass the Europium particle label channel (5) and into the mixing area (4). The Europium labels diffuse in the sample and will bind analytes on their surface. Furthermore, the analyte will bind to the antibodies coated on the surface of the reaction chamber (6). A washing solution is driven from the washing solution chamber (7) to the waste chamber (8). This will remove any particles in the chambers, except the ones specifically bonded to the reaction chamber surface. The fluorescence is measured using a time-resolved fluorimeter and the analyte concentration is derived from these results.

3.2 Manufacturing considerations

The cartridge was fabricated out of high impact polystyrene (PS), using injection molding, thus only this technique will be presented. A metal mold insert, designed in Solidworks®, is used as a replica master for the molding process and was fabricated using

micromilling. An example of a metal mold, used for mixing efficiency studies, in the ReDia project, is presented in Figure 3-2.

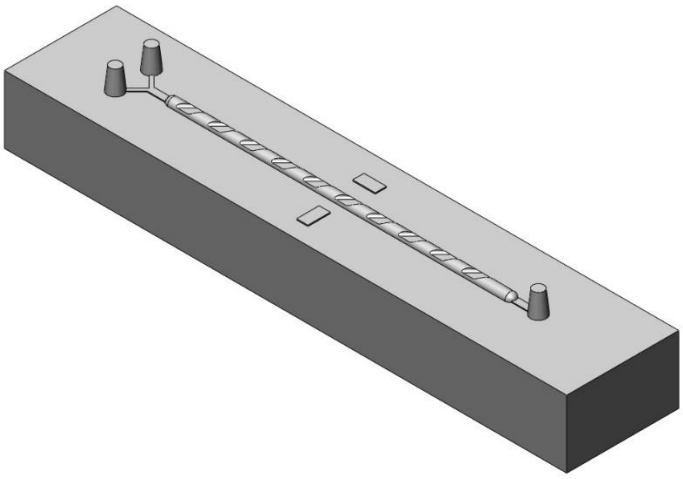

Figure 3-2. *Example of a metal mold insert used in the molding manufacturing process.*

The mold insert was used as a replica for the injection molding process, which consists of four major elements: hopper, screw, sprue and mold insert. An amorphous thermoplastic (here, PS) pellet is loaded in the hopper. The screw shears, melts and pumps the polymer. The polymer is then pushed into the mold through the sprue. Afterwards, pressure is applied and the melt is cooled. Once it solidifies it can be taken out from the mold. A schematic diagram of this process is shown in Figure 3-3 [7].

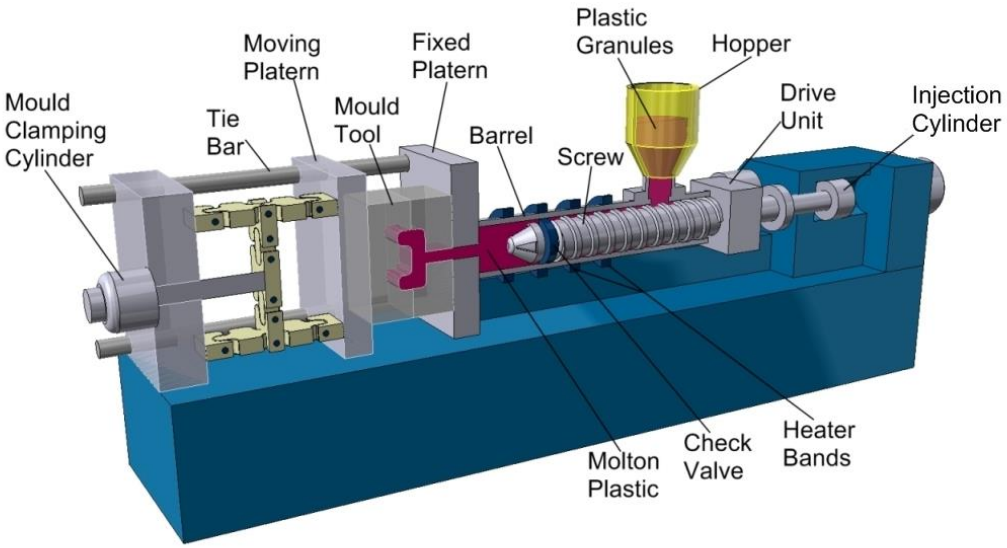

Figure 3-3. *Schematic of injection molding process. Image taken from* ***[31]****.*

After the injection process, the cartridges are sealed using laser transmission welding. Transmission welding offers a contactless bonding of the cartridges, thus avoiding any contamination of the functional areas of the device. Furthermore, it is a fast process, with

high accuracy and good visual properties of the seam. Moreover, there are minimal mechanical and electrical effects on the device, compared to other techniques such as, gluing, lamination, or ultrasonic welding. This is due to the energy generation being highly localized on the welding area. The injection molded plate was bonded to a black extruded PS plate. The black cover was needed, because the laser beam travels through the optically transparent, injection molded piece and is absorbed by the opaque black plate. A durable joint is formed when the materials of both the transparent and the opaque layers melt and then cool down. The welding seam was measured to be approximately 150 μm, with a ±30 μm deviation. [32]

3.3 Mixer Designs

As described in Section 3.1, after the volume metering area, the blood plasma sample is combined with a buffer solution. These two fluids need to be properly mixed before reaching the immunoassay chamber, in order to avoid two main effects that would limit the sensitivity of an immunoassay: the Hook effect and the Matrix effect. The Hook effect occurs when the concentration of an antigen increases past a certain limit. After this limit, even though the antigen concentration increases, the measured antibody-antigen concentration decreases, since all binding sites are occupied. Usually the effect is avoided by diluting the sample into a buffer solution. [33]

The matrix effect occurs due to the sensitivity of the immunoassay to environmental conditions of the sample, called matrix of the sample. The pH level, protein and lipid concentration of the sample affect the reactivity of the antibodies. Since the composition of blood varies quite significantly from one individual to another, the results may be different between individuals, as a result of this effect. Its influence is minimized by diluting the sample into a buffer solution. [33]

The main objective of this work is to design a micromixer that achieves a high mixing efficiency. For this purpose, several micromixer designs are compared in terms of mixing efficiency. Afterwards, a parametric study of the channel parameters is conducted and finally the mixing behavior was confirmed experimentally.

The ReDia project uses a half circular channel of radius 0.5 mm for fluid flow. The selection of this type of channel cross-section was based on it having a lower chance of droplet formation than the rectangular cross-section. Thus, also the micromixer would use this channel. By taking into account the limitations of the injection molding as a manufacturing method, only planar structures could be considered, meaning that structures, such as Figure 2-6 (a) and Figure 2-7 are impossible. Additionally, active micromixers are eliminated, due to their use of an additional source, which would make the micromixer expensive to manufacture and less robust. The remaining micromixer designs, are the lamination based, T- and Y-micromixers, and the chaotic advection based, Serpentine, Slanted Groove and Rips and Staggered Herringbone micromixers.

The micromixer channels used in the simulations has the following general dimensions: half-circular cross-section of radius 0.5 mm and 40 mm channel length. The inlets and outlet are of height h=0.08 mm and width w_{in}= 0.3 mm for inlets and width w_{out}=0.6 mm for outlet. The length of the inlets and outlets is approximately 2.5 mm.

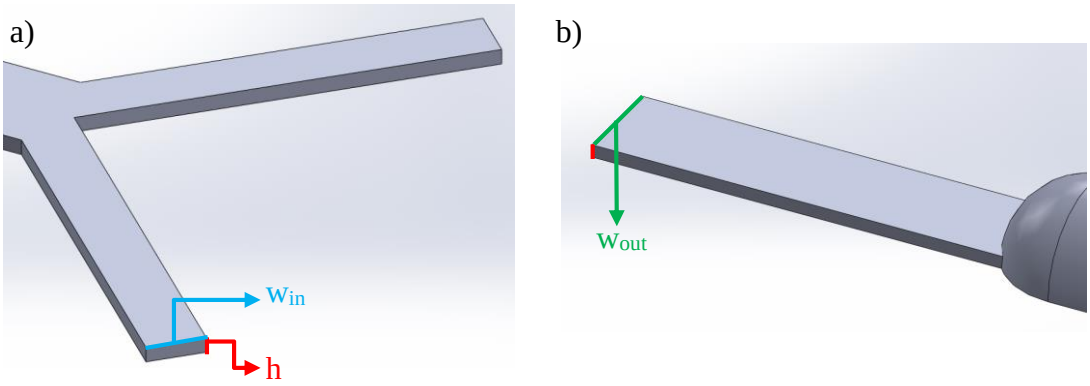

Figure 3-4. *Inlet (a) and Outlet (b) connection dimensions.*

Lamination Micromixers

From the lamination micromixer only the T- and Y-junction micromixers were studied. We did not expect these two micromixers to perform well, and were used only as a base-line for evaluating the other micromixer types. The T-junction can be seen in Figure 3-5 a) while the Y-junction micromixer can be seen in Figure 3-5 b).

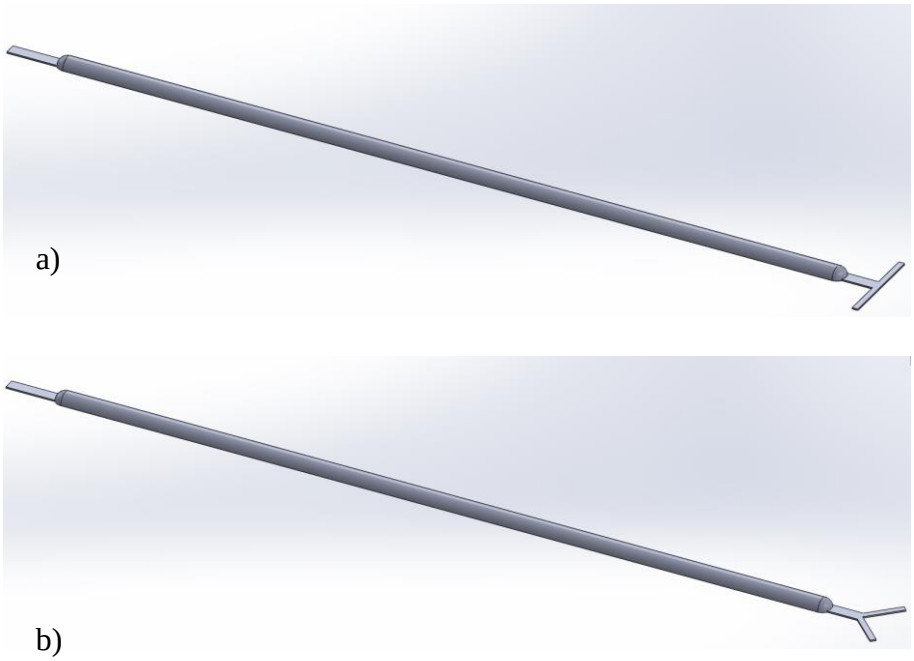

Figure 3-5. *Trimetric view of Typical T-micromixer (a) and Y-micromixer (b).*

The chaotic advection micromixer types studied were: serpentine (Figure 3-6), channel rips (Figure 3-9), channel grooves (Figure 3-7) and herring-bone structures (Figure 3-12). They slight modifications on the structures described in [11] and [19].

Serpentine

The serpentine micromixer is a modification of the zig-zag structure described in [11]**.** The modification was necessary since the zig-zag structure and their sharp turns could produce droplets at the turning points. One such sharp turn is highlighted in Figure 3-6, red box.

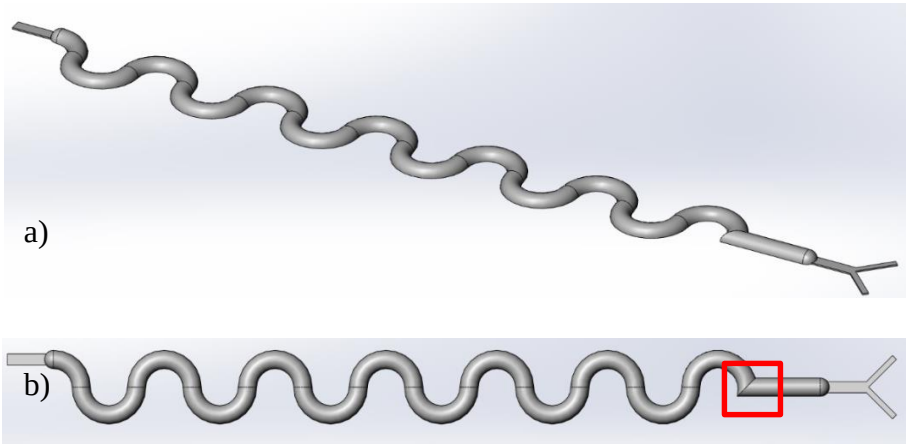

Figure 3-6. Serpentine micromixer. This structure is a modification of the zig-zag micromixer described in *[11]*.

Slanted Groove

The slanted groove micromixer used in this thesis is a modification of the one presented in [11]. Here the groove extend outside the channel, wrapping around it, which is due to the half-circular cross-section.

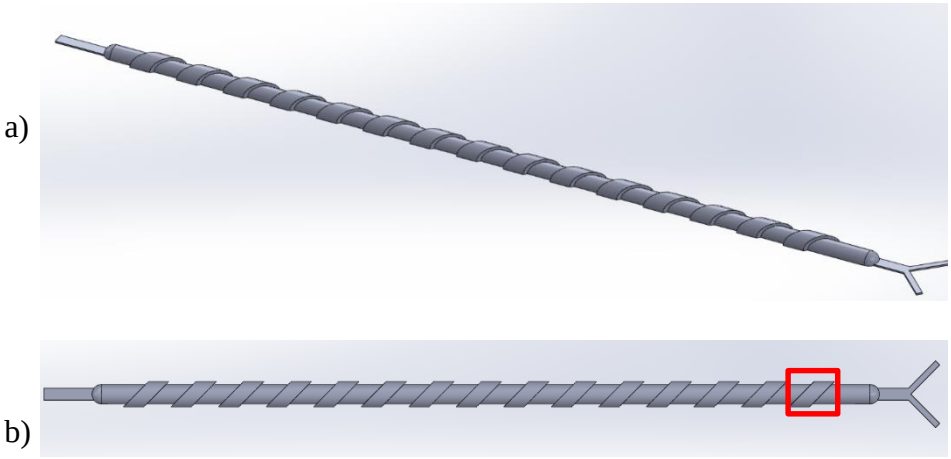

Figure 3-7. *Slanted groove micromixer isometric (a) and top (b) views. Design adapted from* ***[11]****.*

The elements of the groove micromixer (Figure 3-7 b) red box) have a width w=0.75mm and have a height h_e=0.2 mm. The element is extruded with respect to the channel (height

h=0.5 mm). The angle of the elements was a_e=45° and the distance between two consecutive elements was d_e=1mm. The distance between elements was 1 mm. An overview of the dimensions can be seen in Figure 3-8.

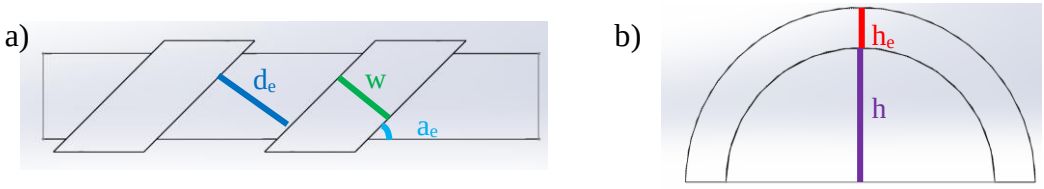

Figure 3-8. *Slanted grooves micromixer element dimensions. View from top (a) and front (b).*

Slanted Rips

The slanted rip geometry, shown in Figure 3-9, is a modification of the slanted rips presented in [11]. The rips are patterned such that they would correspond to a 45° angle cut, with a 0.75 mm wide straight tip at 0.2 mm height (Figure 3-10: a_e, w_e and h_e respectively).

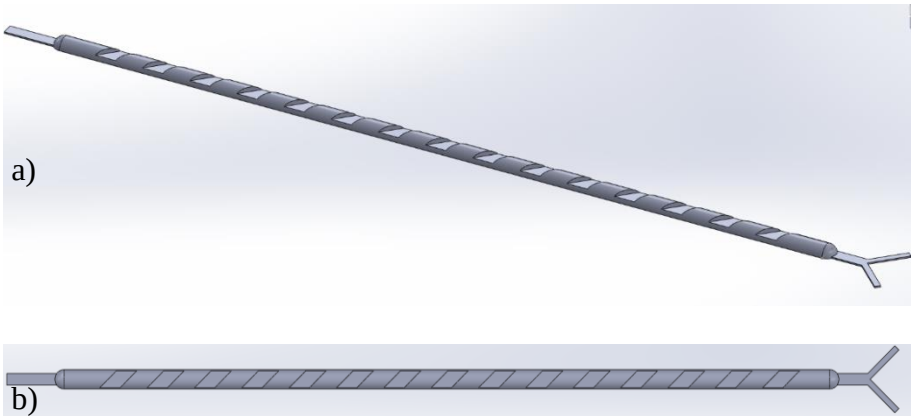

Figure 3-9. *Slanted rips micromixer isometric (a) and top (b) views. Design adapted from* ***[11]****.*

The rips are placed 1 mm apart (Figure 3-10: d_e). A schematic of the dimensions of a rip element is shown in Figure 3-10.

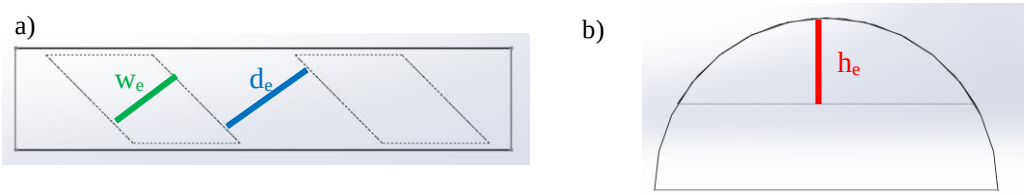

Figure 3-10. *Schematic view of slanted rips elements. a) Top view and b) Front view.*

The rips modified micromixer, shown in Figure 3-11, is a modification of the standard rip. The rip elements are 75% of the length of the standard type.

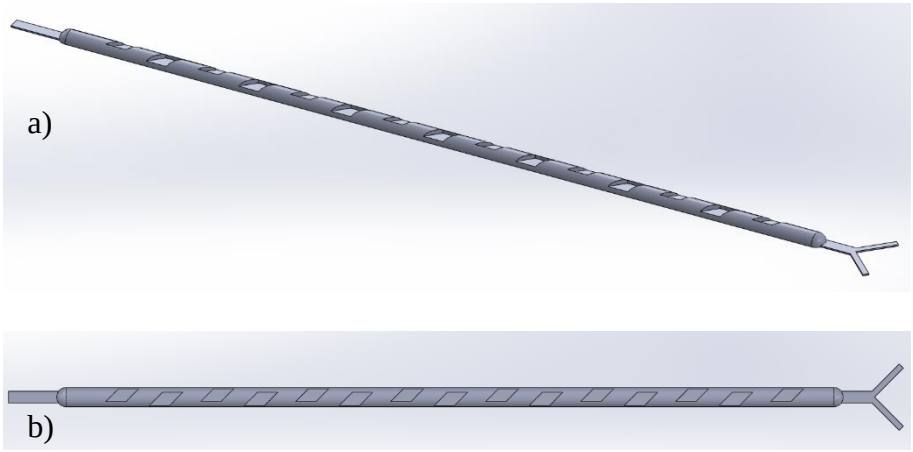

Figure 3-11. *Slanted rips modified micromixer. Design adapted from* ***[11]****.*

Staggered herringbone

The structures, shown in Figure 3-12, represent the typical staggered herringbone micromixer. This micromixer should recirculate the outer fluid flow toward the apex of the structure at each element. The width ratio w_1:w_2 is 2:1 in Figure 3-12, the elements have a 45° angle with the channel wall, a height of h=0.2 mm, and a length of l=0.75 mm.

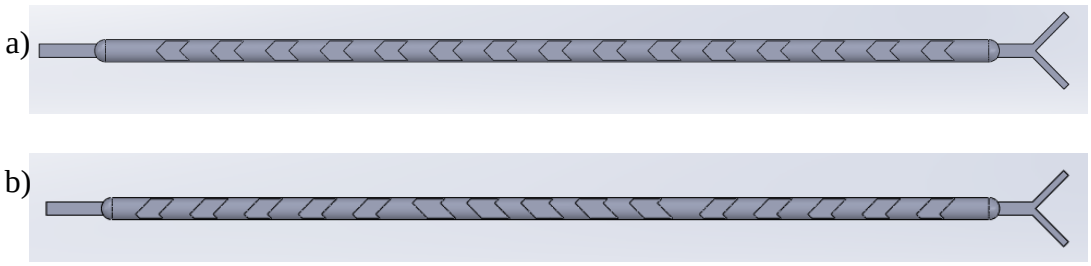

Figure 3-12. *Typical staggered herringbone micromixer. Design adapted from* ***[11]*** *and* ***[19]****.*

[19] and ***[22]*** found that the width ratio w_1:w_2 of 2:1 would be optimal. The apex is defined as the point of intersection between the two sides. In our design it changes position after five elements, thus changing the apex. Since the apex changes position and the flow is recirculated towards the apex, the mixing performance should increase.

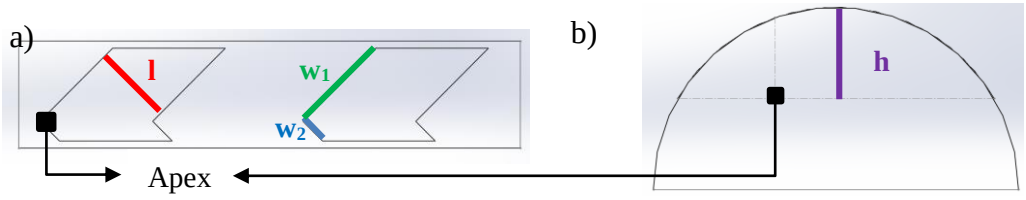

Figure 3-13. *Overview of staggered herringbone micromixer dimensions, described in* ***[19]****. a) Top view; b) Front view*

An overview of the staggered herringbone micromixer dimensions is presented in Figure 3-13. The width (l), height (h) of one element were 0.75 mm and 0.25 mm respectively.

3.4 FEM Modeling

In this thesis, COMSOL was used for FEM modelling of the micromixer geometries. COMSOL Multiphysics is a platform for physics-based modelling and simulation, using advanced numerical methods. It contains dedicated physics interfaces and tools for simulating electrical, mechanical, fluid flow and chemical application, but can also be used for cross-disciplinary models. For each physics, COMSOL solves a unique set of partial differential equations on model boundaries.

The Microfluidics Module of COMSOL used in this work is a collection of tailored physics for simulating the flow in microfluidic devices. The module contains packages, that can be used in modelling laminar or multiphase flows, flows in porous media and rarefied flows. The complexity of the NS equations, make using FEM modelling a necessity. All of the simulations in this thesis were done using the laminar flow package, from which the Single-Phase Flow, Transport of Diluted Species and Particle Tracing physics were used. All studied geometries were designed with a CAD software (Solidworks) and then imported and simulated in COMSOL.

3.4.1 Assumptions

In FEM modelling there are some assumptions made in order to make the computation easier and, in some cases, possible. Generally it is impossible to model blood plasma, as the fluid composition is different from patient to patient and varies with the point where it is measured. Therefore, firstly, the blood plasma was approximated to be a Newtonian fluid ($\rho \approx 1.006e+3$ kg/m^3, $\eta \approx 1.05e-3$ Pa·s). Next, the channel walls were assumed to be smooth, ignoring the defects caused by injection molding and laser welding. Any non-idealities from the pressure source were also ignored, since in some cases, the pressure supply might vary. Lastly, for the particle tracing study, the number of particles released was 200, as opposed to approximately 10^9 particles in the real life scenario.

The assumptions affect the results obtained quite drastically, especially the blood plasma approximation and channel wall smoothness. However, they do not impact the final results and conclusions drawn from the experiments.

3.4.2 FEM Modules used

Single Phase Flow Module

The single phase flow module is used to model the fluid flow inside a channel. The equations solved by this physics are the Navier-Stokes equations (Eq. 1, 3 and 5). The quantity of interest from this physics is the velocity field ($\boldsymbol{v}$). The Transport of Diluted Species and the Particle Tracing physics need initial flow conditions, which are given by the results of this study.

The boundary conditions of the flow model can be split into: wall, inlet and outlet boundaries. The walls have a *no slip* condition, which means that the means velocity field on those boundaries is zero. The inlets have a *pressure, no viscous stress* condition, meaning that on this boundary there is a pressure (p_1). The outlet had a similar *pressure, no viscous stress* condition, however it was set to zero. This means that the pressure at the outlet is zero and the viscous forces are vanishing at the boundary. The conditions are similar to how the pressure differences from inlet to outlet are computed in a *pen-and-paper* analytical model. The resulting velocity field is a function of the position at which the field is evaluated, given by the *x, y* and *z* coordinates. [33]

Transport of Diluted Species Module

This module is used for computing the concentration field of a dilute solute in a solvent. Moreover, the transport and reactions of the species dissolved can be computed. The model assumes that the transport of species is done through diffusion and convection and implements the mass balance equation (Equation 27.).

$$\frac{\partial c}{\partial t} + v \cdot \nabla c = \nabla \cdot (D \nabla c + R) \tag{29}$$

where c is the concentration of species , D is the Diffusion coefficient, R is the reaction rate for species and v is the velocity vector. The velocity vector is taken from the solution of the laminar flow study.

The *no flux* condition is set on the all walls, which means that there is no mass flow in or out of the boundaries. There are two *concentration* boundaries set for the inlets. The outlet has an *outflow* condition, which means that the species are transported out of the model from this boundary. [33]

Particle Tracing for Fluid Flow Module

The particle tracing module is generally used in order to compute the motion of particles within a fluid. Their motion can be driven by drag, gravity or electric, magnetic forces. Here this module was used to evaluate the Europium nanoparticle behavior for the various micromixers studies. The major concern is that the elements of a micromixer might trap the particles. For this module a time dependent analysis is done, where a set number of particles are released, and are driven by flow rate, computed by the single phase flow physics. Moreover, the element impact on the particle trajectory allows us to better understand the flow behavior for various micromixer types.

The physics allows tracing only when the impact of the particles on the flow field is negligible. First one computes the flow field by using the laminar flow physics. Next the motion of the particles is modelled. This is done by applying Newton's second law

$$m\frac{d^2x}{dt^2} = F(t, x, \frac{dx}{dt}), \tag{30}$$

where x is the position of the particle, m is the particle mass and F is the sum of all forces acting on the particle. The only force acting on the particle considered in the model is the drag force, which is the force exerted on the particle due to a difference in velocity between the fluid and the particle. For the studies we used a Stokes drag model:

$$F = \frac{18\eta}{\rho_p d_p^2} m_p (v - u), \tag{31}$$

where v is the flow field and is η the dynamic viscosity, both computed in the laminar flow. This drag model considers as input the density, mass and diameter of the particle as well as the velocity field (u). The particle density (ρ_p) as well as the particle diameter (d_p) were known. The walls had a *bounce* condition set, which means that the particle would be "reflected" upon contact. The Inlet was set to have a 200 particle/release with two releases, one at 0s and one at 0.1s. The Outlet had a *disappear* condition set.

3.4.3 Meshing considerations

Meshing is one of the most important steps in a FEM model. There has to be a compromise between the number of elements in a mesh and the computation times. For the Transport of Diluted Species study a *normal* fluid dynamic mesh is used and is shown in Figure 3-14. The density of the mesh is important since this physics is used to compute the mixing efficiency of a micromixer. On a normal computer (i7, 18 GB DDR3, NVidia Quadro 1000M) the study took around 10-15 minutes. The model used a stationary study.

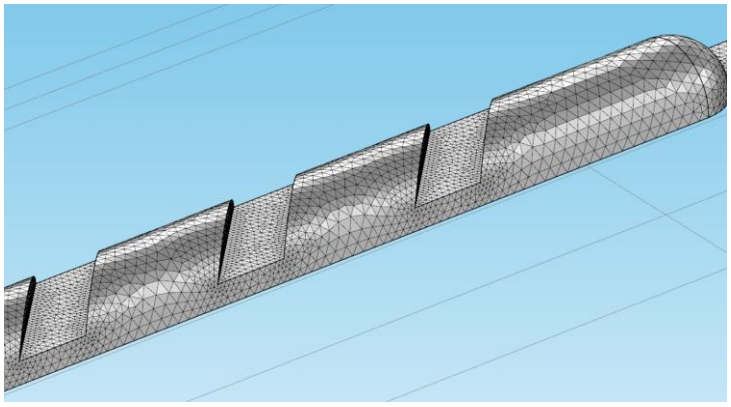

Figure 3-14. *Meshing for the Transport of Diluted species study.*

For the Particle Tracing Module a more coarse mesh is used, shown in Figure 3-15. This is because the result of the study is used to more easily predict the behavior of particles inside the channels, but not in the calculations of the mixing efficiency. The model uses a stationary study to compute the initial values of the geometry, which in this case means

solving the Laminar flow study. The resulting values are then used in a time dependent study of the particle behavior. The mesh used here is a *coarser* mesh type calibrated for fluid dynamics. Using the same setup the study is computed in ~5 minutes.

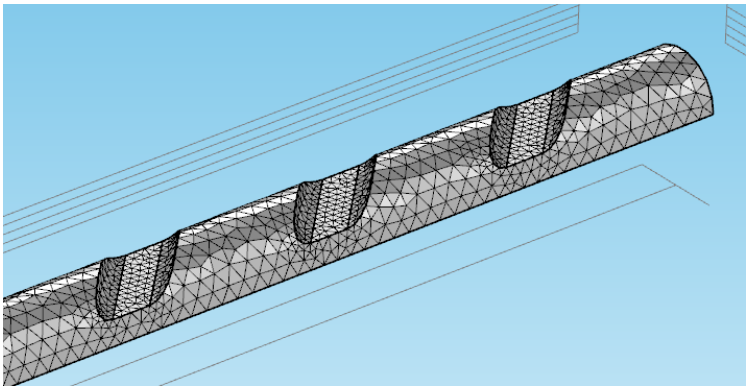

Figure 3-15. *Meshing for Particle Tracing study.*

3.4.4 Mixing Efficiency Evaluation Method

The evaluation of the mixing efficiency of a structure is done by quantifying the concentration fields at two boundaries: inlet and outlet. As mentioned there are two different conditions for the inlet boundaries. One inlet is set to have an initial concentration (c0, shown in Figure 3-16a) red box) while the other inlet has an initial concentration of 0. At each evaluation boundary, including the inlet and outlet, we compute the concentration variance. This is done by subtracting the computed concentration (c_{inlet} or c_{outlet}) from the concentration when the two fluids are perfectly mixed (which is $c_0/2$), and then squaring the result. By dividing the concentration variance at the outlet to the concentration variance at inlet we obtain a dimensionless variable (S, Equation. 28), that allows us to quantify the mixing efficiency of a micromixer.

$$S = \frac{\left(c_{outlet} - \frac{c_0}{2}\right)^2}{\left(c_{inlet} - \frac{c_0}{2}\right)^2}; S \in [0,1] \tag{32}$$

Figure 3-16 shows how the evaluation of the mixing efficiency is evaluated in COMSOL. The concentration is calculated at each point in the mesh (Figure 3-16 a) using Equation 29. The computed concentration belongs to the interval [c_0, 0] (concentrations at each inlet). When plotting the concentration on a surface, 'c_0' will be shown as red, '0' blue, and the average of them as light green (Figure 3-16 b) left, right and center areas, respectively. The variance, computed as described above, is synonymous to the degree of uniformity of the concentration at the evaluation surface. For extremely efficient mixing, the concentration variance at the outlet should be close to the $c_0/2$. This corresponds to a uniform distribution of the light green area (similar to Figure 3-16 c). When evaluating

the mixing efficiency, if S=1 the two fluids have not mixed at all, while if S=0 the two fluids are perfectly mixed. Generally, one is looking for a micromixer where the number S is lowest.

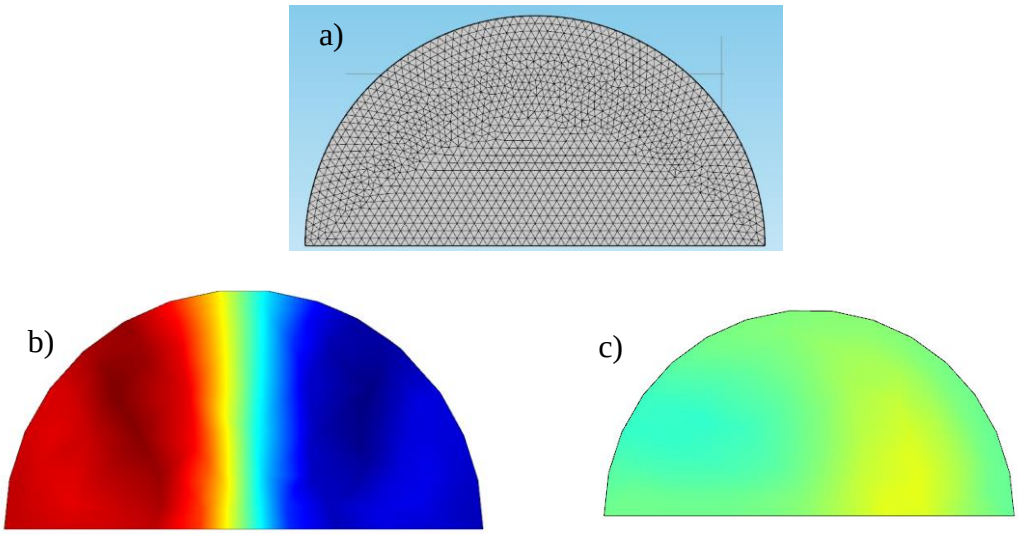

Figure 3-16. *Inlet and Outlet views in COMSOL for the slanted groove micromixer. a) Inlet and Outlet Mesh; b) Concentration at Inlet; c) Concentration at Outlet.*

Figure 3-17 shows the evaluation boundaries for the inlet and outlet concentration variances. The red box in Figure 3-17a) illustrates the inlet boundary, which has the initial concentration set to c_0, while the other inlet has the concentration set to 0.

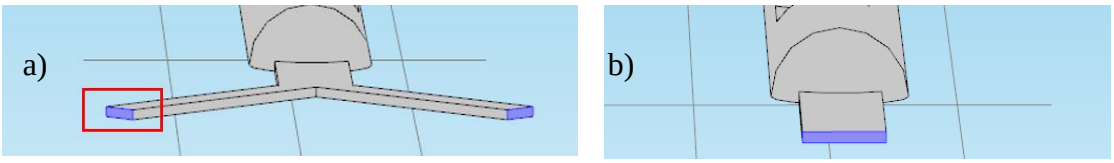

Figure 3-17. *Boundaries used for evaluating the mixing efficiency of a micromixer. Here the slanted rips (Figure 3-9) is used: a) inlets b) outlet.*

3.4.5 Modeling Cases

The micromixer types, described in Section 3.3, are evaluated in terms of mixing efficiency, using the method described in 3.4.4, with a Transport of Diluted Species model coupled with a Single Phase Flow one. However, two other factors that need to be considered when selecting a particular micromixer. First of all, when selecting a micromixer, the manufacturing complexity plays an extremely important role. There is no reason to select an extremely efficient micromixer, if the manufacturing complexity and thus, costs are too high. Secondly, the probability of air droplet formation, by either the channel geometry or the elements of the micromixers, needs to be taken into account. Although the mixing is important, the functionality of the immunoassay has a more important role

in the project. Air droplet were found to have tendency to block the inlet of immunoassay, and thus considerably reducing its sensitivity, or rendering it useless. [34]

By taking all of these factors into account, the most suitable micromixer design is further examined, by conducting a parametric study. Parameters such as, channel length, inlet pressure and, for chaotic advection micromixer, element geometry, influence the mixing efficiency quite drastically. In this study, one of these parameters is varied and the mixing efficiency is computed, while all other parameters are kept constant. For each parameter a Transport of Diluted Species model is coupled with the Single Phase flow model and the mixing efficiency is evaluated according to 3.4.4. Similarly, there are other factors which influence the parameter selection, apart from the mixing efficiency. Again, the manufacturing costs and the air droplet formation play and important role in choosing a particular parameter.

After the most suitable combination of parameters from the parametric study is chosen, a particle tracing model is used to simulate the behavior of the Europium nanoparticles inside the micromixer. Of special interest here is the interaction between the nanoparticles and the channel wall and, for chaotic advection micromixers, the interaction with the elements. The purpose of this study is to gain more insight into the behavior of the particles and to evaluate if any would get trapped by the micromixer elements.

3.5 Experimental Validation

Similar to the experimental validation methods described in 2.4, two colored DI-water solutions were used, one dyed with blue food color, the other with a yellow food color, in order to confirm the mixing behavior of the micromixers from the simulation. The difference in the general composition between the food colors allows for a qualitative assessment of the mixing method. Moreover, the air droplet formation for blood plasma samples in the micromixer was studied. The setup consisted of a syringe pump (NE-501, New Era Pump Systems), CCD camera (Sony XCD-X70).

4. RESULTS AND DISCUSSION

This section contains the main results obtained from the COMSOL simulations, as well as the experimental validation part. Firstly, the different mixer types described in Section 3.3 are tested. The mixing efficiency is evaluated as previously described. Next, a parametric study is conducted for the micromixer that yielded the best results. In addition, a particle tracing study is carried out, in order to observe the behavior of the fluid within the micromixer. Lastly, the experimental validation of the simulations is carried out, as described in Section 3.5.

4.1 Micromixer types

For this study the general parameters were: 40 mm channel length, 0.5 mm radius- half circular geometry. The inlet pressure used for all micromixers was 4 mbar. The parameters for this simulation were chosen in order to approximate real-case conditions as closely as possible. For the more complex geometries the element dimensions are provided in Section 3.3. The geometries were modeled in COMSOL using the steps described in Section 3.4.

In order to better observe the behavior of the fluids within each type of micromixer *yz* plane slices (cross-sectional slices) were taken out from each mixer at *x*= 1. 9, 19, 29, 39 mm. For the chaotic advection micromixers, additional *yz* (top-bottom) and *xy* (side-section) plane slices were taken, in order to provide a better understanding of the mixing behavior and are illustrated in Appendix B. There was no reason to use the *xz* and *xy* plane slices for the diffusion based micromixers, as the mixing should only be based on diffusion and there would be little to no change in the concentration shown in the images.

For all structures an isometric view of the mixing behavior is shown in Appendix A. For the chaotic advection types the transparency of the isometric view is turned on. This would correspond to the image taken from a CCD camera in real life and the fluid behavior can be more easily observed. Similarly, there was no reason to have the transparency enabled for the diffusion based micromixers, as the view seen from the top part would be almost constant at any point in the structure.

4.1.1 T-Junction

The first study was carried out on the most common lamination mixer, the T-Junction micromixer. Normally, one does not expect an extremely efficient fluid mixing, but the T-junction can serve as a baseline for the mixing efficiency of other structures.

As expected the two fluid only mix through diffusion. The diffusion 'boundary' is located in the center, which is visible in Figure 4-1. For this micromixer type the concentration variance at outlet was 0.4598. As mentioned before a mixing efficiency of 1 would mean that the fluids are completely un-mixed, while a mixing efficiency of 0 would mean perfect mixing. Though diffusion only, after 40 mm, the fluids are approximately half-mixed.

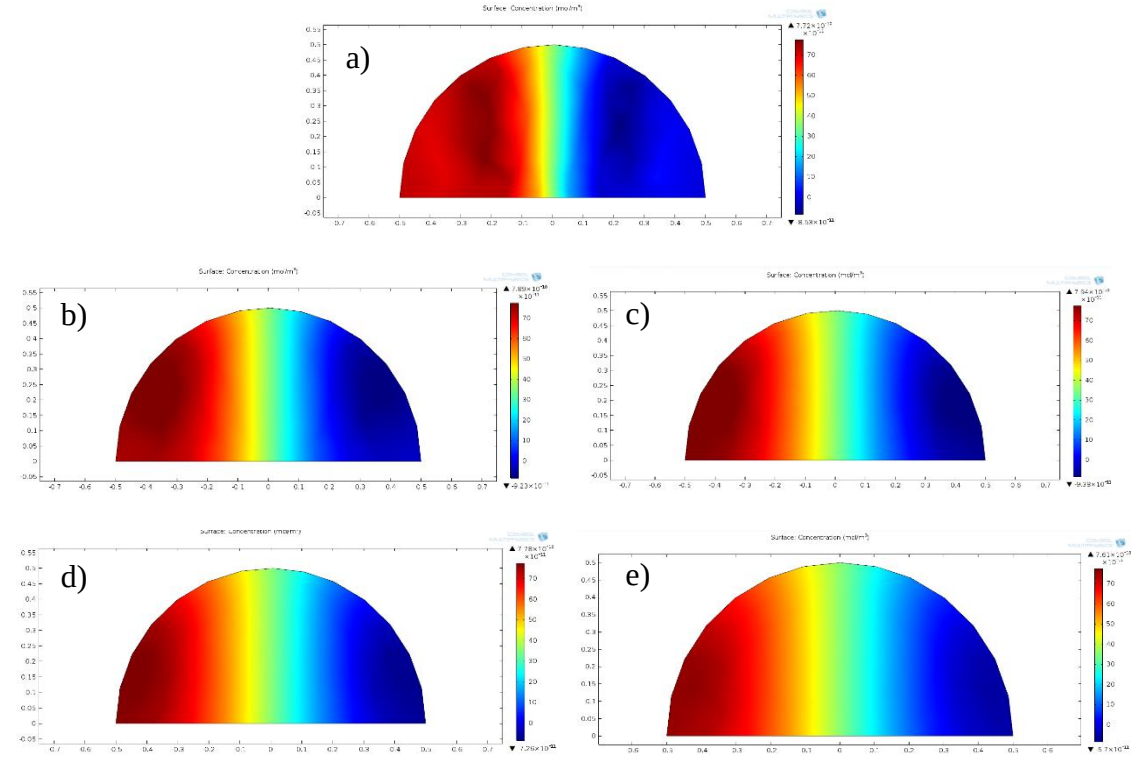

Figure 4-1. *yz- plane slices of the T-junction micromixer at x: a) 1 mm; b) 9 mm; c) 19 mm; d) 29 mm; e) 39 mm.*

4.1.2 Y-Junction

Similar to the T-Junction, the Y-Junction micromixer should mix the fluids through diffusion. Figure 4-2 shows the diffusion between the two fluids at different lengths. Here the concentration variance at outlet was 0.4640.

From this we can conclude that all chaotic micromixers should have a lower mixing efficiency that both T- and Y-junction types. For all other micromixer either a T- or a Y-junction type inlet could be used. We selected the Y-type, since it has a lower chance of producing air droplet at the merging point.

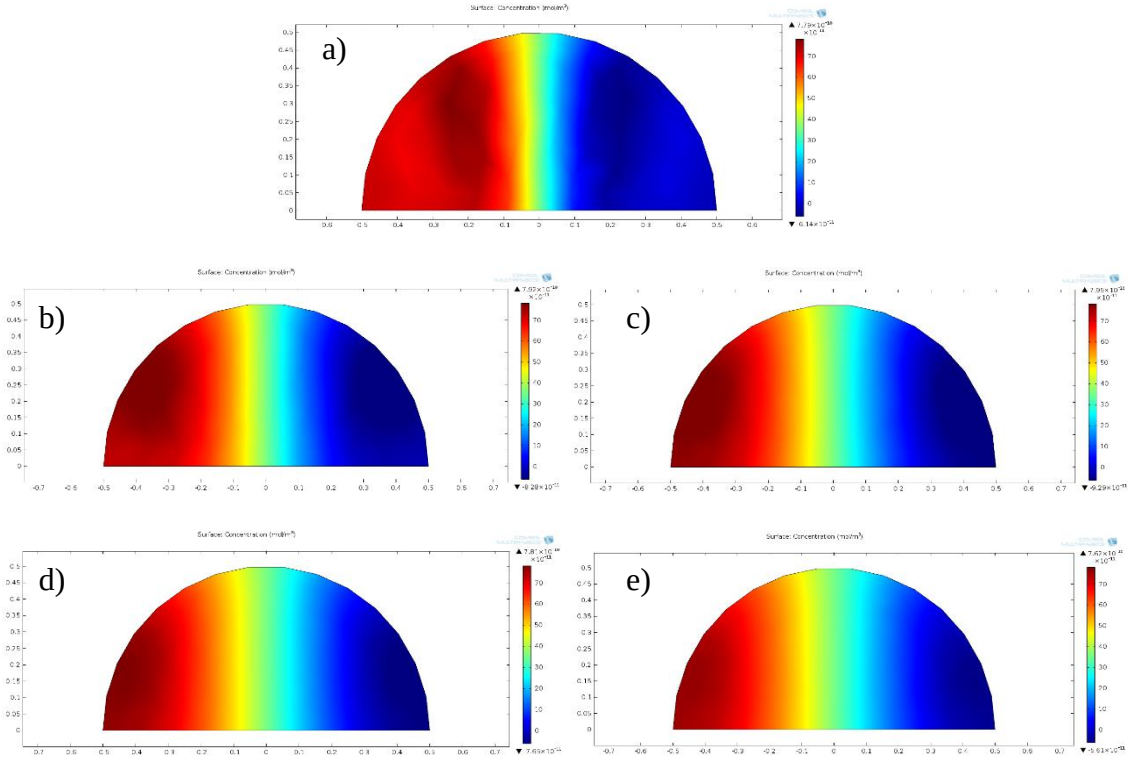

Figure 4-2. *yz- plane slices of the Y-junction micromixer at x: a) 1 mm; b) 9 mm; c) 19 mm; d) 29 mm; e) 39 mm.*

4.1.3 Serpentine

The first chaotic advection micromixer was the Serpentine micromixer. Figure 4-3 shows the fluid mixing at different lengths. Similar to the T-junction and the Y-junction geometries the mixing is done only by diffusion. Even though the structure is part of the chaotic advection types, in our case it behaves as a lamination micromixer. This is, most likely, due to the small pressure used to propagate the flow, which is not enough to induce chaotic advection. Although the structure mixes only based on diffusion, it is more effective than the T- and Y-junction types, since the concentration variance at outlet was 0.3095.

The biggest problem with the serpentine mixers is the effective area which they occupy. For example the effective area of a Y-junction micromixer is ~120 mm^2, while the designed serpentine would have a 240 mm^2. A general requirement of the microfluidic cartridge was that all components (sample inlets, volume metering, mixing, washing, waste chambers and the immunoassay) should ‘fit’ inside a 50x55 mm^2 rectangle. Thus, any micromixer, from the designed structures, that yields a better mixing efficiency than the serpentine should be a better option.

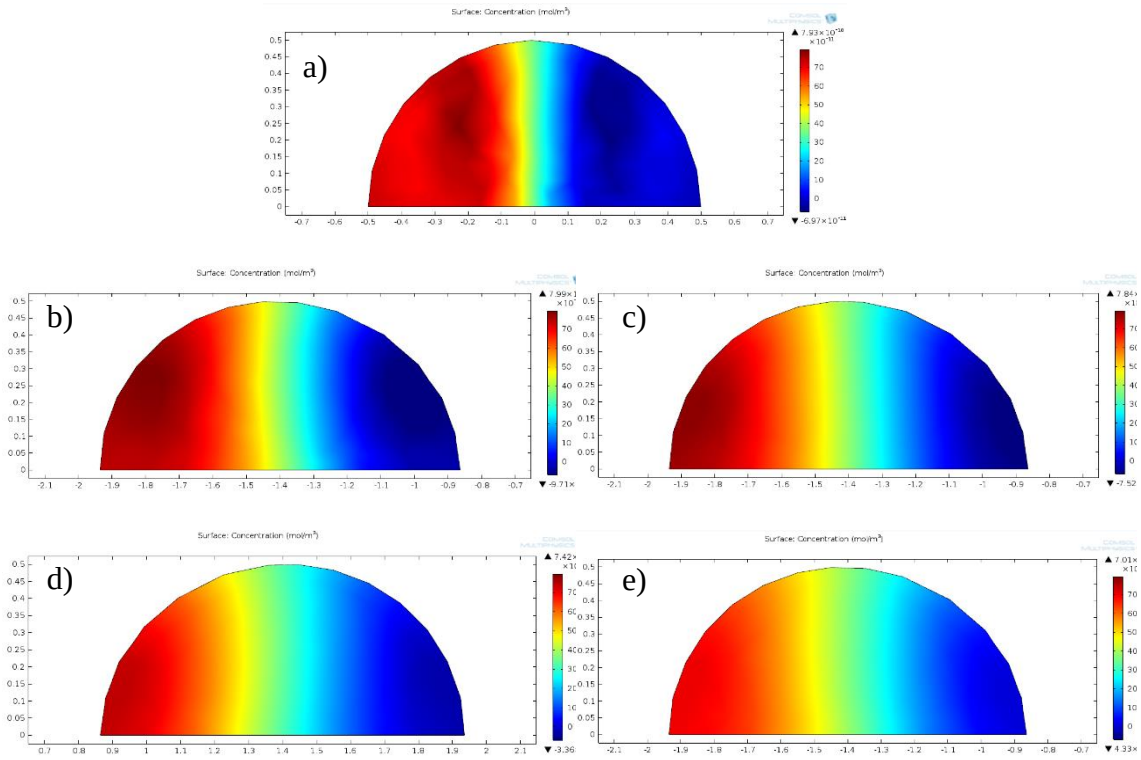

Figure 4-3. *yz- plane slices of the serpentine micromixer at x: a) 1 mm; b) 9 mm; c) 19 mm; d) 29 mm; e) 39 mm.*

4.1.4 Grooves

The flow behavior is dependent on the groove parameters and the number of grooves. The groove parameters are described in Section 3.3. Figure 4-4 shows the flow behavior along channel length. We can observe that the flow is recirculated (twisted) towards the left side, along the groove orientation. This increases the contact area between the two fluids, producing a much more effective mixing than the lamination type. This is also confirmed by the results, where the groove structures yielded a concentration variance at outlet of 0.0996.

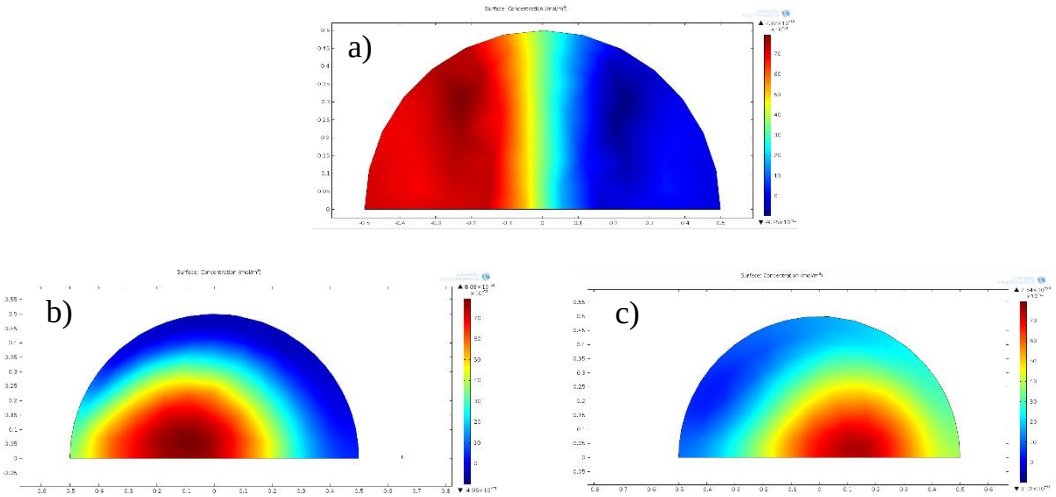

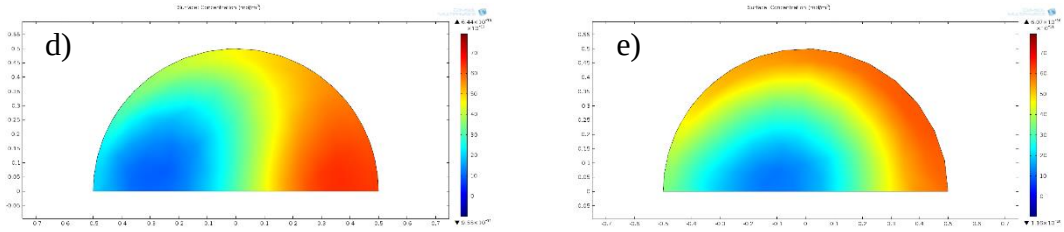

***Figure 4-4**. yz- plane slices of the groove micromixer at x: a) 1 mm; b) 9 mm; c) 19 mm; d) 29 mm; e) 39 mm.*

4.1.5 Slanted Rips

Similar to the groove micromixer, the slanted rips should recirculate and 'twist' the flow, and increase the contact area between the two fluids. The general dimension of a rip element can be found in Section 3.3. The position of the two fluids changes, seen in Figure 4-5.*b*, *c* and *d* where the position of the blue fluid alternated from top to bottom, and from right to left. Although the rips behave similarly to the grooves geometry (flow recirculation along the rip orientation), the mixing efficiency is higher in the slanted rip case. This can be also be seen when comparing Figure 4-4.*e* and Figure 4-5.*e*, which represents the outlet view in each case. The fluids are more uniformly mixed in the second case, seen in the intensity values of the two fluids. Light green would represent perfect mixing.

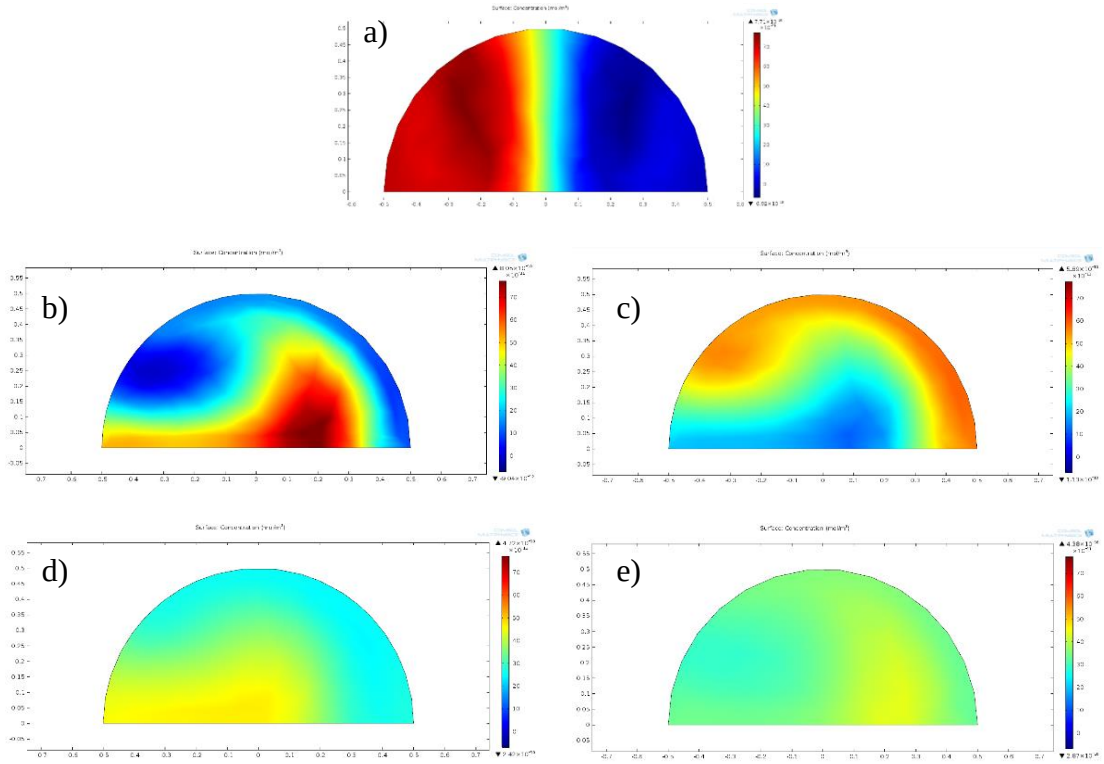

***Figure 4-5.** yz-plane slices of the Rips micromixer at x: a) 1 mm; b) 9 mm; c) 19 mm; d) 29 mm; e) 39 mm.*

The concentration variance at outlet yielded by the rip micromixer was 0.0111 which is ten times lower, and thus better, than the groove micromixer.

4.1.6 Slanted Rips Modification

Similar to the slanted rip and grooves previously presented, the slanted rip modification geometry should recirculate and 'twist' the flow according to the direction of the rip. The difference here being that the flow would be partially recirculated since, theoretically, the flow should be unaltered if the rip is not present. This should make the mixing more efficient than the typical rip case. An overview of the rip dimensions can be found in Section 3.3.

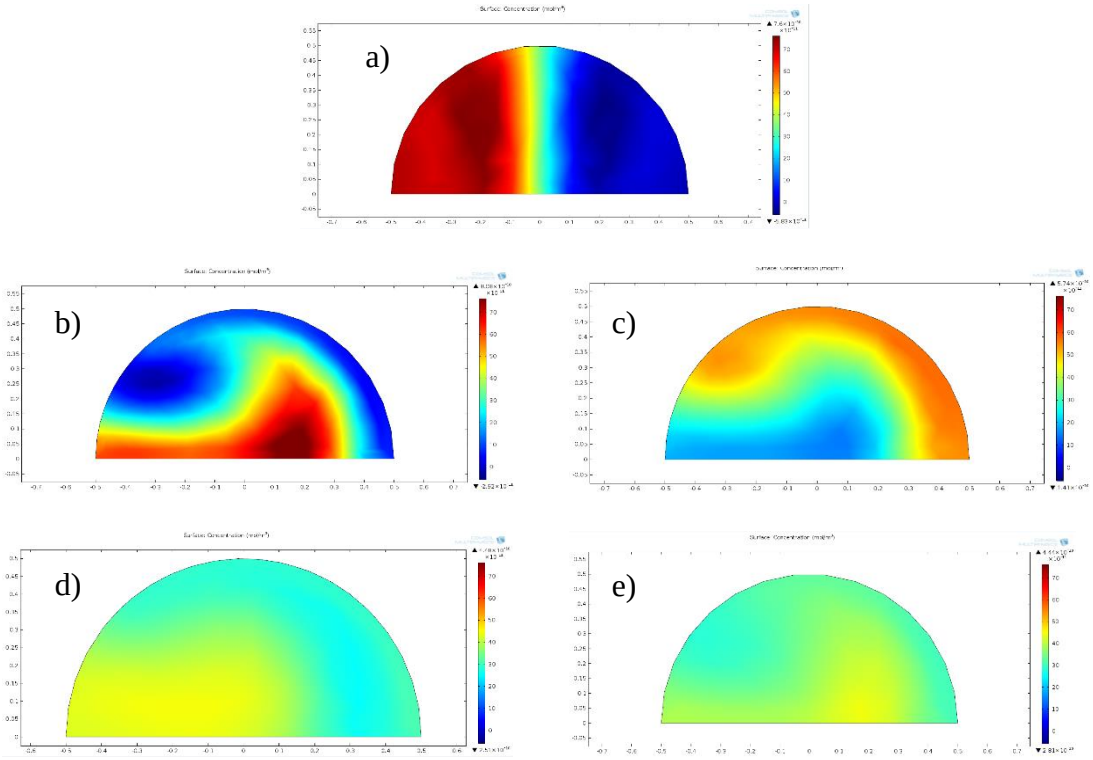

Figure 4-6. *yz- plane slices of the modified Rips micromixer at x: a) 1 mm; b) 9 mm; c) 19 mm; d) 29 mm; e) 39 mm.*

The results showed that there is no partial recirculation of the fluids, the micromixer behaving similar to the typical slanted rip micromixer. Moreover, the concentration variance at outlet was computed to be 0.0824, which is much worse than the typical rips structure, but comparable to the efficiency obtained by the groove structure. Figure 4-6 shows the mixing at different points in the channel. Visually the results are also worse than the rips geometry. This can be easily observed by comparing Figure 4-5.*e* and Figure 4-6.*e*.

4.1.7 Herringbone

The herringbone micromixer is one of the most studied chaotic advection micromixers. It has been shown that the design allows for the best micromixing results. [11] Here, we used a five herringbone-element groupings, with three herringbone-groups. The dimensions of one herringbone element in the grouping can be found in Section 3.3.

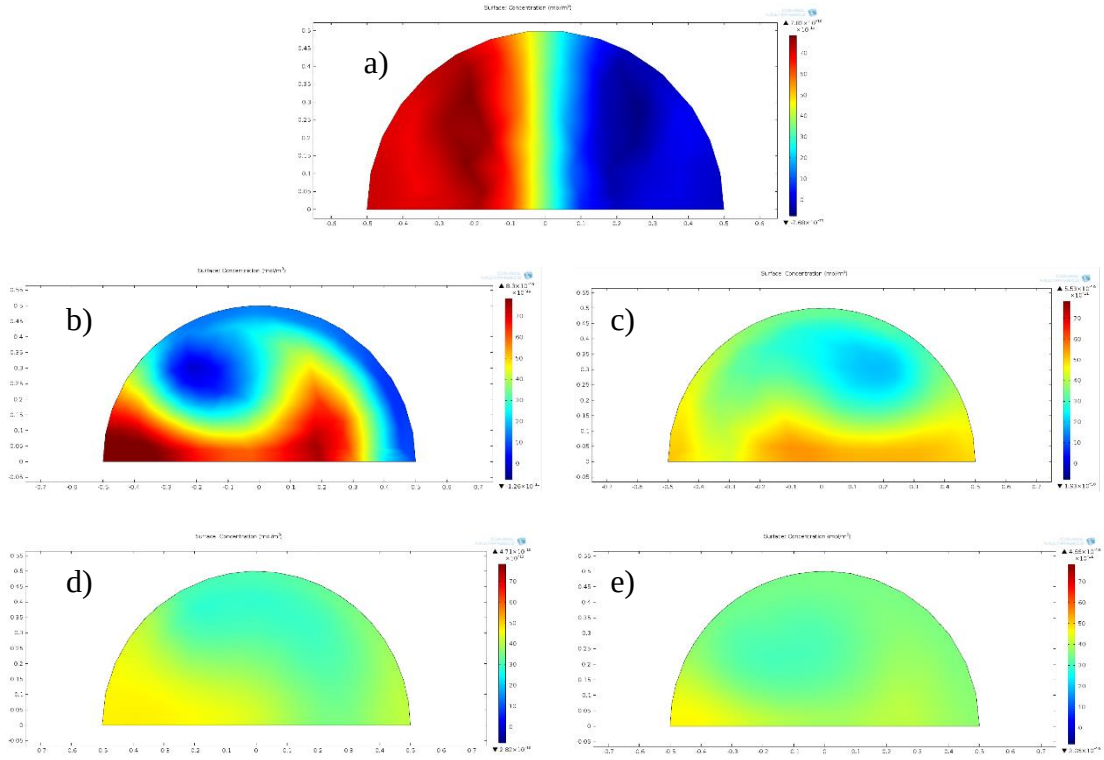

Figure 4-7. *yz- plane slices of the Herringbone micromixer at x: a) 1 mm; b) 9 mm; c) 19 mm; d) 29 mm; e) 39 mm.*

Theoretically, the flow should be focused towards the apex and recirculated. This can be seen in Figure 4-7.*b) - e)*, where the apex position alternates, depending on the apex position in the geometry. The 9 mm (*b)* slice corresponds to the first herringbone grouping, the 19 *(c)* mm and 29 mm *(d)* to the second grouping, while the 39 mm *(e)* slice correspond to the outlet, after the last five element grouping. The concentration variance at outlet was computed to be 0.0048, which is twice as good as the rips structure.

4.1.8 Herring Bone Modification

Even though literature states that the herringbone geometry is optimal when the width ratio is 2:1, it also depends on the application. Since, here we have a half circular cross section, rather than the typical rectangular one, the last studied chaotic micromixer has a width ratio of 1:1. A full overview of the dimensions of this micromixer can be found in Section 3.3.

This means that the flow should be recirculated towards the middle, where the apex is positioned. Visually the two flows seem to be still unmixed, seem by the amount of light green, which indicates prefect mixing. Quantitatively, the concentration variance at outlet was 0.0948 which is ten times higher than the rips geometry.

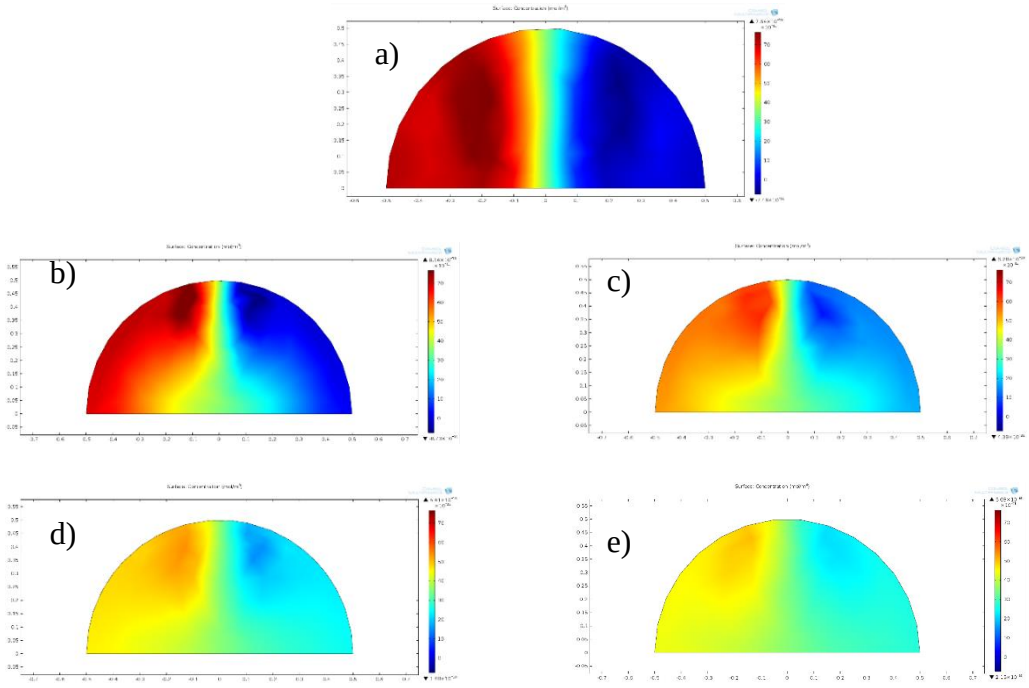

Figure 4-8. *yz- plane slices of the modified Herringbone micromixer at x: a) 1 mm; b) 9 mm; c) 19 mm; d) 29 mm; e) 39 mm.*

4.1.9 Analysis of the Micromixer type results

This section contain a summary of the results from Sections 4.1.1 - 4.1.8. Table 1 shows the different concentration variances at outlet of different micromixer types. We can easily see that the typical rips and herringbone structures perform the best. Purely based on the concentration variance at outlet the herringbone structure should be used, as it yields the best mixing efficiency. However, two other factors needed to be considered when selecting a particular micromixer.

First of all, when selecting a micromixer the manufacturing complexity plays an extremely important role. There is no reason to select an extremely efficient micromixer if the manufacturing complexity and thus costs are too high. From the presented chaotic advection micromixers, the slanted rips structure is the easiest to manufacture. The diffusion based micromixers presented are extremely easy to manufacture, but their efficiencies are too low to be considered.

Table 1. *Concentration variance at outlet of different micromixer geometries*

Geometry	Concentration Variance
T-mixer	0.4598
Y-mixer	0.4640
Serpentine	0.3095
Grooves	0.0996
Rips	0.0111
Rips Modification	0.0824
Herringbone	0.0048
Herringbone Modification	0.0948

As mentioned previously, another factor when selecting a micromixer is the probability of air droplet formation. The immunoassay functionality is more important than the mixing efficiency. Thus, any geometry that minimizes the chances of air droplet formation should be chosen, even at the cost of a lower mixing efficiency. The minimization of droplet formation, is done by eliminating any geometry with sharp edges, corners, turns either in the flow path or on the channel walls, where air pockets can be formed or trapped. The typical and modified herringbone have a higher chance of producing droplets, since they have sharp edges in the flow path and at the apex of the structures. Similarly, the modified slanted rip geometry is quite susceptible to droplet formation, since the rip element ends in the flow path of the fluids. There needs to be a compromise between the mixing efficiency, manufacturing cost and droplet formation. From this perspective the slanted rips geometry is the best option, as it has the second highest mixing efficiency (second lowest concentration variance), while having the low probability of droplet formation and a medium manufacturing complexity and cost. Thus, only the slanted rip structure is studied further.

The isometric view for all structures is presented in Appendix A, providing an overview of the mixing behavior of each micromixer. Appendix B shows a comparison between the slanted rips, modified slanted rips and herringbone structures. For each structure xz slices were taken at y= {-2.5, 0, 2.5} mm and xy slices were taken at z= {0.1, 0.2, 0.4} mm. The figures confirm the conclusions previously drawn from the respective geometry results and also illustrate the different mixing behavior of the micromixers presented.

4.2 Parametric Study of the Slanted Rips Micromixer

Here, the element width, element height, inlet pressure and channel length are varied in order to determine the optimal configuration.

4.2.1 Width and Height Change

In this experiment the element width and height parameters were varied. The element width range was from 0.5 to 1.25 mm with 0.25 mm steps. The element height was varied between 0.15 mm to 0.35 mm with 0.05 mm step size. The spacing between two consecutive elements was kept constant at 1 mm. Figure shows the results of this study.

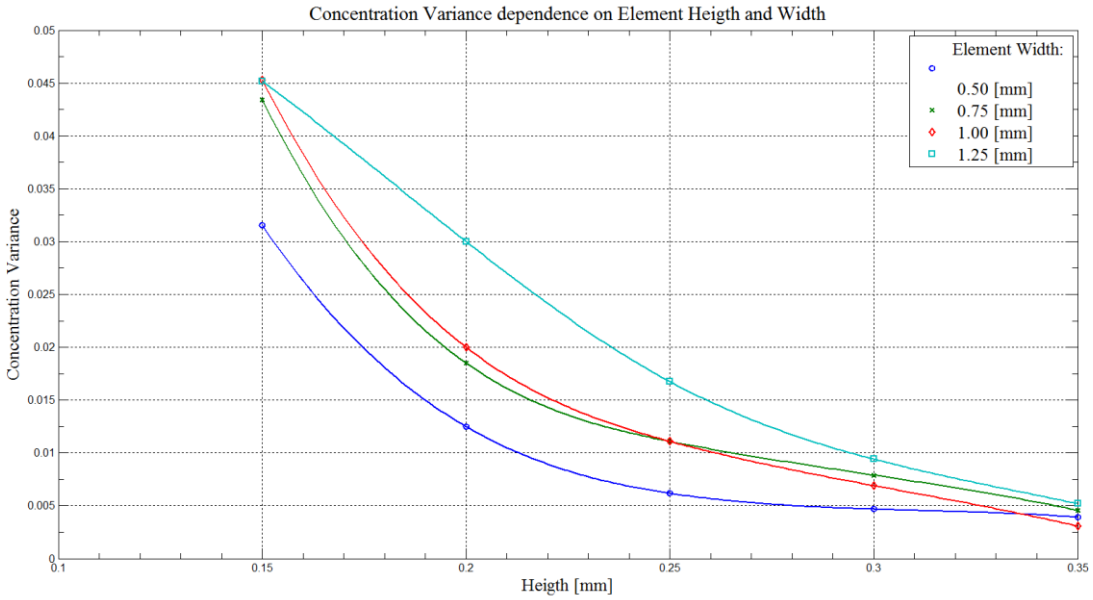

Figure 4-9. *Concentration variance dependence on element width and height.*

We can observe that a smaller element width yields a smaller concentration variance and thus a higher mixing performance. A smaller element width, results in more elements that can be patterned in the same channel length. Furthermore, a larger element height yields a smaller concentration variance and produces better mixing. For the slanted rip geometry the flow is forced, by the element, towards the bottom of the channel before the mixing element. After the flow passes the mixing element, it will be forced towards the channel top and is shown in Figure 4-10.

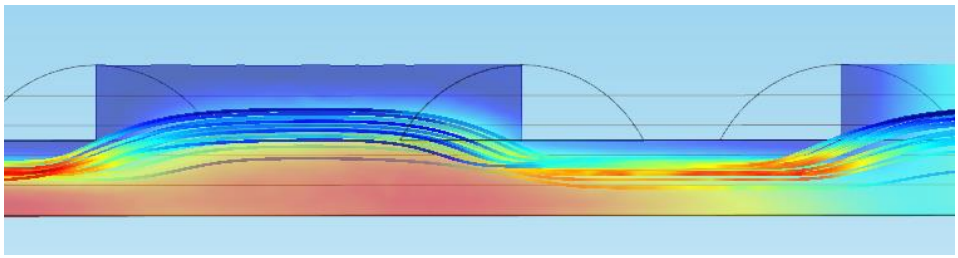

Figure 4-10. *Velocity profile of the xz plane at y=0 mm. Velocity vector is shown as a streamline and the concentration is plotted on the cross-section.*

From this study, we can conclude that a smaller element width and a larger element height combination produces the best mixing results. However, similar to the previous section, there are some other factors determining the parameter selection. For the element height, both the 0.35 and 0.3 mm were excluded, since they could act as a passive valves, blocking the flow. In order to prevent this, higher pressure would be needed. However, since we are dealing with blood plasma, higher pressures might produce air droplets inside the channel. Moreover, the element itself could act as a wall, trapping some air pockets in the region after the element and the channel upper wall. For these reasons we selected the 0.25 mm height.

In terms of the element width, the 0.5 mm structures were excluded since they would increase the manufacturing cost. This is because a smaller tip would be needed to make the metal insert rip patterns. Smaller tips are more expensive and tend to break more easily. As the concentration variance is almost identical for the 0.75 mm and 1 mm cases, we decided to use the 1 mm one.

Similarly, there is a chance of air droplet becoming trapped between the elements and the upper wall. In order to minimize this the corners were rounded. Essentially, any of the rip elements could be done by using a 0.25 mm radius tip which would cut the channel at a 45° angle, at 0.25 mm height. The structure is presented in Figure 4-11.

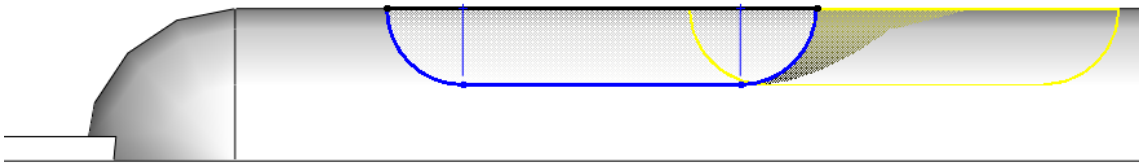

Figure 4-11. *Schematic of rounded rip element. The sketch is then used to cut the half-circular channel (yellow line).*

4.2.2 Pressure Change

The purpose of this study was to investigate the effect of pressure on the concentration variance. The pressure control of the microfluidic cartridge was intended to be active. For example, for the volume metering area, it was found that a minimum of three pressure steps are required for the structure to work as intended. The pressure steps were 8 mbar initially, then 10 mbar and finally 12 mbar. In terms of micromixer, the outlet pressure of the volume metering area (12 mbar) could be used. However, since there is active control of the pressure, smaller values could be used as well. Essentially, any pressure that would be high enough to propagate the flow from the inlet to the outlet of the micromixer, could be used. It was impossible to calculate the minimum pressure needed for this, as the pressure is dependent on the flow speed, and thus the flow rate. Figure 4-12 shows the dependence of the concentration variance on inlet pressure. A 3.25 ml/min flow rate was found to be maximum in the immunoassay measurements [34]. This corresponds to approximately 1.85 mbar pressure for a 40 mm long, straight channel. By taking into account the pressure drops induced by the slanted rips, the lower pressure was set to 4 mbar. Both the upper and lower pressure values are only needed to give an indication of the mixing efficiency dependence, so as to select the more appropriate value in real measurements.

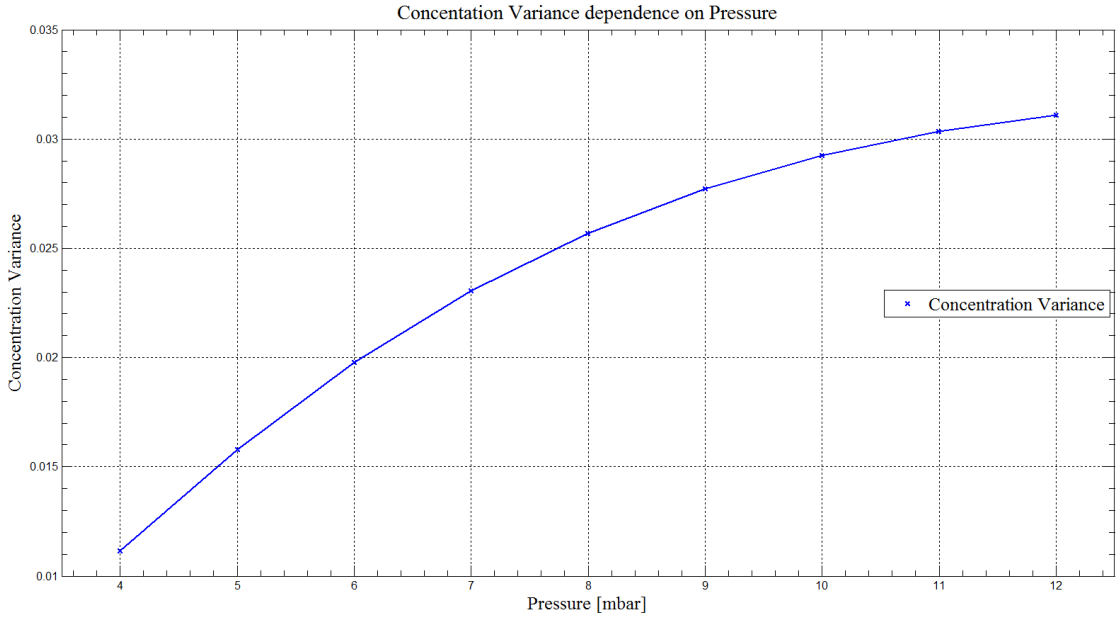

Figure 4-12. *Concentration variance dependence on inlet pressure.*

As we can easily observe, the concentration variance increases with pressure. This means that, theoretically, a smaller pressure should be used. However, lower pressures mean that the total time needed for the sample to reach the immunoassay and thus, to obtain the result increases. Again, there should be a compromise between the total time spent for the

fluid to reach the immunoassay (which depends on the pressure) and the mixing efficiency. Ideally, the time required to the immunoassay to display results should not be increased by other components.

4.2.3 Channel Length Change

The purpose of this study was to investigate the concentration variance dependence on channel length. Initially the 40 mm channel length was selected since that would correspond to the maximum channel length usable in the cartridge. The cartridge has a 50 mm length, out of which at least 5 mm from each side should not be used in order to avoid channel leakage due to imperfect bonding. Another option is to have turns (see Figure 4-13), thus increasing the effective length of the micromixer beyond the 40 mm limit. The structure could also have rips patterned onto it.

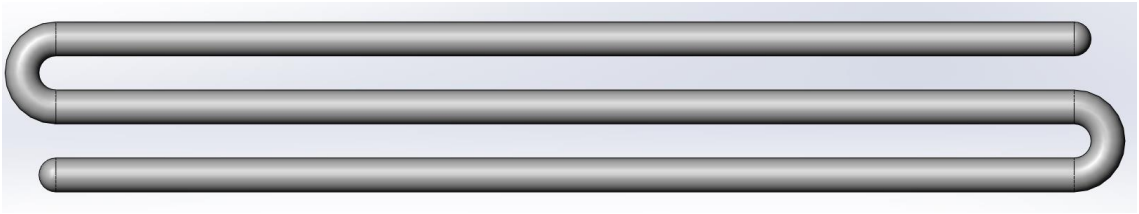

Figure 4-13. *Example of micromixer with turns.*

Figure 4-14 shows the concentration variance dependence on channel length. The inlet pressure was 4 mbar and the rip dimensions were as described in Section 3.3 for the slanted rips geometry.

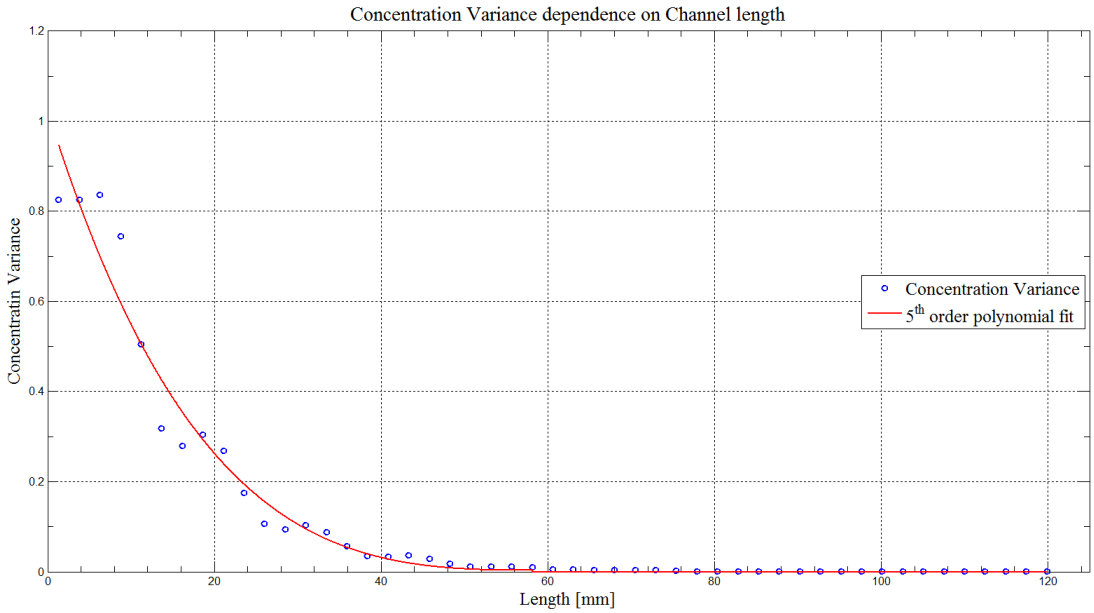

Figure 4-14. *Concentration variance dependence on channel length.*

From Figure 4-14, we can conclude that any mixer longer than 40 mm would yield extremely good mixing. In the final geometry, a mixer with an overall channel length of approximately 60 mm was used.

4.2.4 Analysis of the Parametric Study Results

Although there are several studies that investigate the mixing efficiency dependence on the channel and element parameters, they are focused towards the slanted grooves and herringbone micromixers, [20-29]. To the authors' knowledge, there is no study done on the slanted rip geometry and the parameters' effect on the mixing efficiency. The parameter that seems to influence the mixing efficiency of the slanted rip micromixer is the element height, where the mixing efficiency improves by approximately 90% at each height step. The second parameter, in terms of importance, is the element width, which improves the mixing efficiency by 60% at each step. The pressure increases the mixing efficiency by 50% at the first pressure step and by 3% at the last pressure step. The channel length initially increases the efficiency by 320% from 0 to 20 mm, by 200% from 20 to 40 mm and only by approximately 10% afterwards.

The selection of the final parameters, which were used further is based on other factors except the mixing efficiency, as mentioned in the previous sections. Even though a more efficient combination of parameters exists, for this particular application a 0.25 mm element height, 1 mm element width, with rounded edges of 0.25 mm radius and 30 mm channel length, were chosen.

4.3 Particle tracing

The particle tracing study was done in order to observe the Europium nanoparticle behavior when they encounter the channel rip. More importantly the particle should not stick to the channel walls. For the study, a 12 mbar pressure was used. The rip parameters were 0.25 mm height, 1 mm width with rounded edges (0.25mm radius). The parameters were identical to the ones used in the final geometry. Initially all the particles are on the inlet wall. After approximately 0.1 seconds the particles reach the first rip. There, they are initially pushed down towards the bottom and then twisted according to the orientation of the groove (here towards right, Figure 4-15 a)). As an example, suppose a particle is initially in the center, top of the channel. When it is near the rip, it will start to move downwards. After it passes the rip its position is now almost at the bottom, right hand wall**.** At this point other particles are at the top, center of the channel wall. The process is repeated for each rip. The particle tracing experiment revealed that no particles are trapped on the rip walls and moreover, they do not get stuck after the rip.

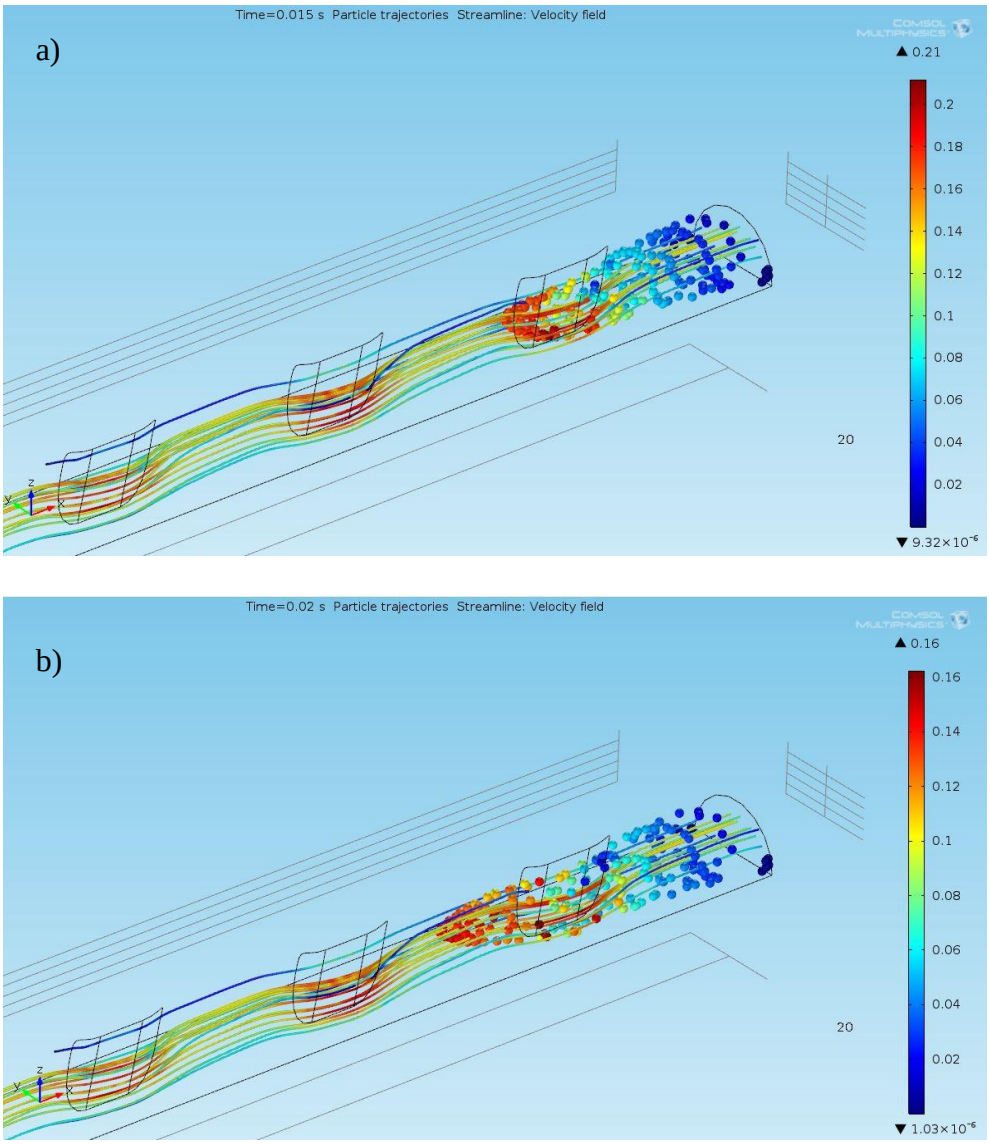

Figure 4-15. *Particle tracing results; Particles at: a) 0.015s b) 0.025s*

4.4 Experimental validation

For performing the experimental validation, a micromixer insert was designed (Figure 4-16). Based on the results previously presented in 4.2, the micromixer had a 30 mm length with slanted rip elements patterned as described in 4.2.4. The length was chosen to be 30mm, since the insert needed to have enough room for inlet and outlet placement. Moreover, a dead-area of 2mm, from each side, was needed in order to allow for laser welding and manufacturing imperfections. The mixing efficiency for a 30 mm long channel was found sufficiently high. The metal insert was then used for injection molding.

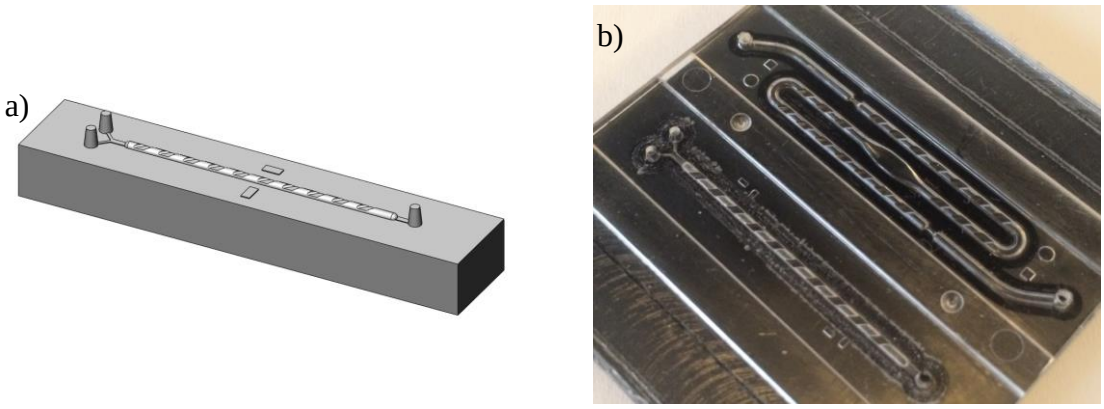

Figure 4-16. *a) Micromixer insert design. b) Welded insert used in micromixing and immunoassay tests*

The experiment was performed by pumping two colored DI-Water solutions (blue and yellow). A syringe pump was used to provide flow rate. The purpose of the study was to confirm the fluid behavior in the micromixer predicted by the FEM models. For this reason the flow rates used here have no relevance.

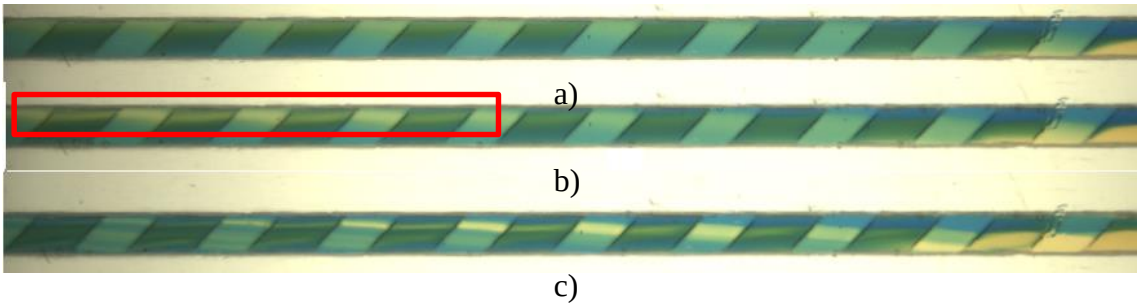

Figure 4-17. *Micromixer at different flow rates: a) 12.5 µl/min; b) 25 µl/min and c) 50 µl/min.*

Figure 4-17 shows that the fluid revolves with the rips. This is more apparent in the second case, where the fluids change places: initially yellow is at bottom, finally (red box) it is at the top. Similar to the FEM model, Figure 4-18, after a number of rips the two fluid change positions. This is further confirmed by Figure 4-17 c), where we can easily observe layering of the fluids, together with interchanging of layers.

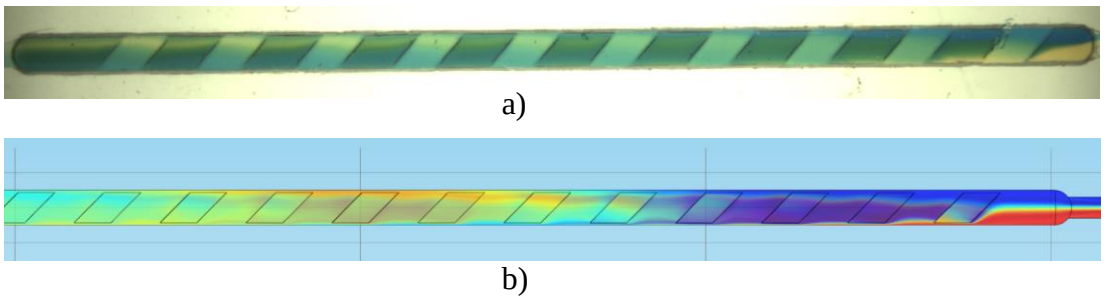

Figure 4-18. *Real (a) vs. Simulation (b) results top view.*

When comparing the simulation results (Figure 4-18 b) with the experimental results (Figure 4-18 a) we can observe that the micromixer behave in a similar manner. This is further

confirmed by Figure 4-19 where a close-up view of the first rip is presented. The layering of the fluids, present in Figure 4-17 c), occurs only at high flow rates in real cases, however they confirm the layering from Figure 4-19 b).

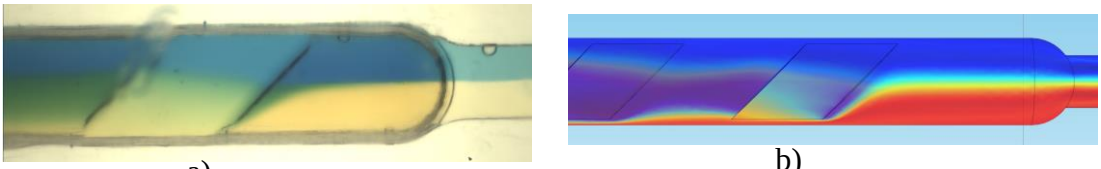

a) b)

Figure 4-19. *a) Real and b) Simulated close up view of the first rip element.*

The insert was also tested with blood plasma to investigate the air droplet formation. Although droplets generally do not form**,** in the rare case where droplets appeared, they were trapped between the rip elements. This means that they will not block the immunoassay, but will just render one rip element useless. As mentioned earlier, these experiments were only used to confirm the simulation results. For the blood plasma tests no images are provided, since without any dye the plasma is not visible enough to be imaged.

5. CONCLUSION

The thesis shows how finite element method modelling can be used to design new geometries for the microfluidic immunoassays. The method allows the solving complex differential equations, which can be used to describe a simplified version of a system.

There is limited knowledge on the behavior of micromixers, especially for the chaotic advection types. From this category the most studied geometry is the staggered herringbone micromixer. However, real-world constraints have to be taken into account when studying the mixing efficiency of a micromixer, such as manufacturing cost and complexity, droplet formation probability or cartridge/channel related criteria.

This thesis studied several passive micromixers. From the developed FEM models, purely based on mixing efficiency, it was found that the herringbone structure achieved the highest mixing efficiency. Despite this, due to the real-world constraints, the slanted rip micromixer was better suited for this particular application. In addition, for the slanted rips structure, a parametric study was conducted, in order to determine an optimal parameter configuration, which allows for extremely efficient mixing. It was found that the slanted rip element height and width were the two most important parameters, as their mixing efficiency increases drastically with the increase in height and decrease in length. Despite this, a smaller element height of 0.25mm (0.35mm maximum) was chosen, due to the possibility air droplet formation and element acting as a passive valve, and a larger element width of 1 mm (0.75mm minimum) was chosen, due to lower manufacturing costs.

The evaluation of the mixing efficiency is done by evaluating the concentration variance at the outlet, which is similarly defined to the ones available in literature. To the authors' knowledge, it is the only true quantitative method of evaluating the mixing efficiency in simulations. Moreover, currently, there is no study on the parameter influence on the mixing efficiency for the slanted rip micromixer. Almost all studies focused on optimizing an extruded herringbone micromixer patterned on a channel with a rectangular cross-section.

Thus, it can be concluded that even though a particular micromixer performs better, purely in terms of mixing efficiency, it might not be suitable for the intended application, when real-case constraints are applied. The concentration variance evaluation method is an extremely good indicator of the mixing efficiency of micromixer. Even though there are more sophisticated experimental validation techniques such as confocal fluorescence microscopy, imaging the mixing of two slowly miscible fluid with a CCD camera accurately proves the fluid mixing behavior from the simulations.

REFERENCES

[1] EDMA - diagnostics for health, "About In Vitro Diagnostics," [Online]. Available: http://www.edma-ivd.be/index.php?page=About-In-Vitro-Diagnostics. [Accessed 15 08 2018].

[2] Capital Health, "Pathology and Laboratory medicing - Point of care testing," Capital health, [Online]. Available: http://www.cdha.nshealth.ca/pathology-laboratory-medicine/clinical-services/point-care-testing. [Accessed 15 08 2015].

[3] Markets and Markets, "Point of care diagnostic market," Markets and Markets, September 2014. [Online]. Available: http://www.marketsandmarkets.com/Market-Reports/point-of-care-diagnostic-market-106829185.html. [Accessed 20 08 2015].

[4] C. D. Chin, V. Linder and S. K. Sia, "Commercialization of microfluidic point-of-care diagnostic devices, Critical Review," *Lab on a Chip*, vol. 12, pp. 2118-2134, 2012.

[5] M. MacPherson and M. Ravichandiran, "Lab-on-a-chip technology: the future of point-of-care diagnostic ability," *University of Western Ontario Medical Journal*, vol. 80, no. 1, pp. 24-27, 2011.

[6] H. Bruus, "Chapters 2, 3, 5 and 7," in *Theoretical Microfluidics*, New York, Oxford University Press, 2008, pp. 19-31; 37-63; 91-98; 123-127.

[7] N.-T. Nguyen and S. Wereley, "Chapters 2, 3 and 9," in *Fundamentals and Applications of Microfluidics*, Boston, Artech House, 2002, pp. 11-62; 67-118; 386-401.

[8] J. Berthier and P. Silberzan, "Chapters 2 and 6," in *Microfluidics for Biotechnology, Second Edition*, Norwood, Artech House, 2010, pp. 17-70; 265-271.

[9] S. D. Senturia, in *Microsystem Design*, New York, Springer Science+Business Media, 2001, pp. 103-106.

[10] Biolinscientific, "Static and dynamic contact angles and their measurement techniques, Theory Note 1," [Online]. Available:

http://www.biolinscientific.com/attension/applications/?card=AA7. [Accessed 04 April 2015].

[11] N.-T. Nguyen and Z. Wu, "Micromixer - a review," *Micromechanics and mircroengineering,* vol. 15, no. 2, pp. R1-R16, 2005.

[12] G. S. Jeong, S. Chung, C.-B. Kim and S.-H. Lee, "Applications of micromixing technology," *Analyst,* vol. 135, no. 3, pp. 460-473, 2010.

[13] L. Capretoo, W. Chang, M. Hill and X. Zhang, "Micromixing within Microfluidic Devices," in *Microfluidis: Technologies and Applications*, Berlin, Springer-Verlag, 2011, pp. 27-68.

[14] A. D. Stroock and e. al, "Chaotic Mixer for Microchannels," vol. 295, no. 5555, pp. 647-651, 2002.

[15] J. Lee and S. Kwon, "Mixing efficiency of a multilamination micromixer with consecutive recirculation zones," *Chemical Engineering Science,* vol. 64, pp. 1223-1231, 2009.

[16] A. Alam and K.-Y. Kim, "Mixing performance of a planar micromixer with circular chambers and crossing constriction channels," *Sensors and Actuators B: Chemical,* vol. 176, pp. 639-652, 2013.

[17] V. Hessel, H. Lowe and F. Schonfeld, "Micromixer - a review on passive and active mixing priciples," *Chemical Engineering Science,* vol. 60, no. 8-9, pp. 2479-2501, 2005.

[18] COMSOL, "COMSOL - Lamella Mixer," 2015. [Online]. Available: http://www.comsol.com/model/lamella-mixer-466. [Accessed 12 08 2015].

[19] S. P. Kee and A. Gavriilidis, "Design and characterisation of the staggered herringbone mixer," *Chemical Engineering Journal,* vol. 142, no. 1, pp. 109-121, 2008.

[20] I. Sabotin, G. Tristo, G. Bissacco, M. Junkar and J. Valentincic, "Staggered Herrinbone Mixer designed for micro EDM milling," *Journal of Microelectronics,* vol. 43, no. 1, pp. 3-13, 2013.

[21] Y. Du, Z. Zhang, C. Yim, M. Lin and X. Cao, "Evaluation of Floor grooved Micromixers using concentration-channel length profiles," *Micromachines,* vol. 1, pp. 19-33, 2010.

[22] D. Hassell and W. Zimmerman, "Investigation of the convective motion through a staggered herringbone micromixer at low Reynolds number flow," *Chemical Engineering Science,* vol. 61, pp. 2977-2985, 2006.

[23] W. Jeon and B. Shin, "Design and simulation of passive mixing in microfluidic systems with geometric variations," *Chemical Enginnering Journal,* vol. 152, pp. 572-582, 2009.

[24] S. Hossain, M. Ansari and K.-Y. Kim, "Evaluation of the mixing performance of three passive micromixers," *Chemical Engineering Science,* vol. 150, pp. 492-501, 2009.

[25] R. J. Shilton, L. Y. Yeo and J. R. Friend, "Quantification of surface acoustic wave induced chaotic mixing-flows in microfluidic wells," *Sensors and Actuators B: Chemical,* vol. 160, pp. 1565-1572, 2011.

[26] L.-M. Fu, "Chaotic vortex micromixer utilizing gas pressure driving force," *Chemical Engineering,* vol. 214, pp. 1-7, 2013.

[27] T.-S. Sheu, S. J. Chen and J. J. Chen, "Mixing of a split and recombine mixer with tapered curved microchannels," *Chemical Engineering Science,* vol. 71, pp. 321-332, 2012.

[28] C. Johnson, in *Numerical Solution of Partial Differential Equations by the Finite Element Method*, Dover Publications, 2009, pp. 9-13; 67-83.

[29] B. W. Zimmerman, in *Multiphysics Modeling with Finite Element Methods*, World Scientific Publishing Co. Pte. Ltd., 2006, pp. 1-26.

[30] COMSOL, "Finite Element Analysis (FEA) Software," COMSOL, 2015. [Online]. Available: http://www.comsol.com/multiphysics/fea-software. [Accessed 10 08 2015].

[31] J. Tell, "Teel enginnering - How to Manufacture a product," [Online]. Available: http://teelengineering.com/how-to-manufacture-a-product/. [Accessed 11 08 2015].

[32] A. Mantymaa, H. Jussi, V. Lasse and P. Kallio, "The effects of laser welding on heterogeneous immunoassay performance in a microfluidic cartridge," *Biomicrofluidics* , vol. 5, no. 4, pp. 046504-046504- 11, 2011.

[33] COMSOL, "The Chemical Species Transport Branch, The Fluid Flow Branch," in *COMSOL Multiphysics User's Guide,* 2012, pp. 652-669; 670-704.

[34] J. Valiaho, "M.Sc. Thesis, Improving performance of a Microfluidic immunoassay using a finite element method modelling," Tampere University of Technology, Tampere, Finland, 2012.

[35] F. K. Hansen, "Information on Contact Angle," Rame-Hart, September 2010. [Online]. Available: http://www.ramehart.com/contactangle.htm. [Accessed 04 April 2015].

APPENDIX A: ISOMETRIC SLICES OF VARIOUS CHAOTIC ADVECTION MICROMIXERS

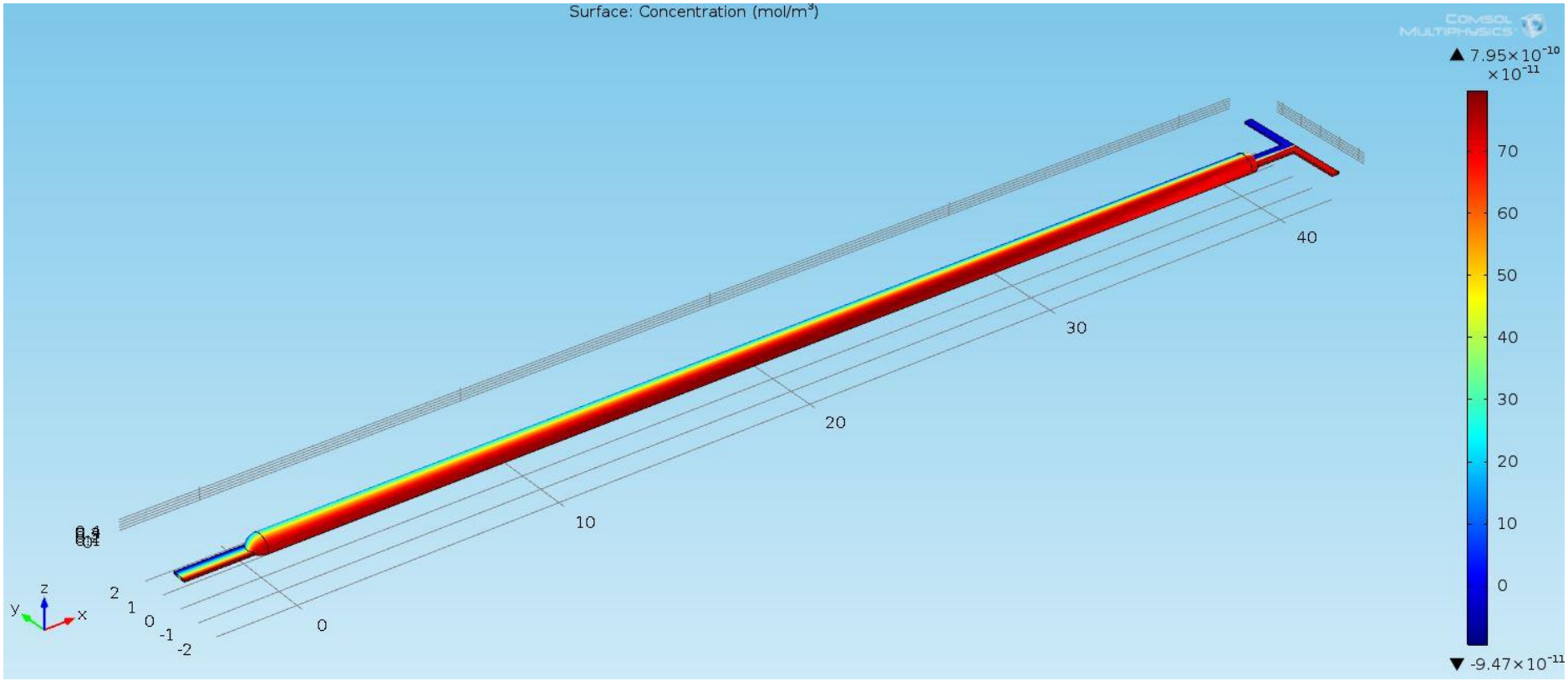

Figure A-1. *Isometric view of the mixing in the T-junction micromixer.*

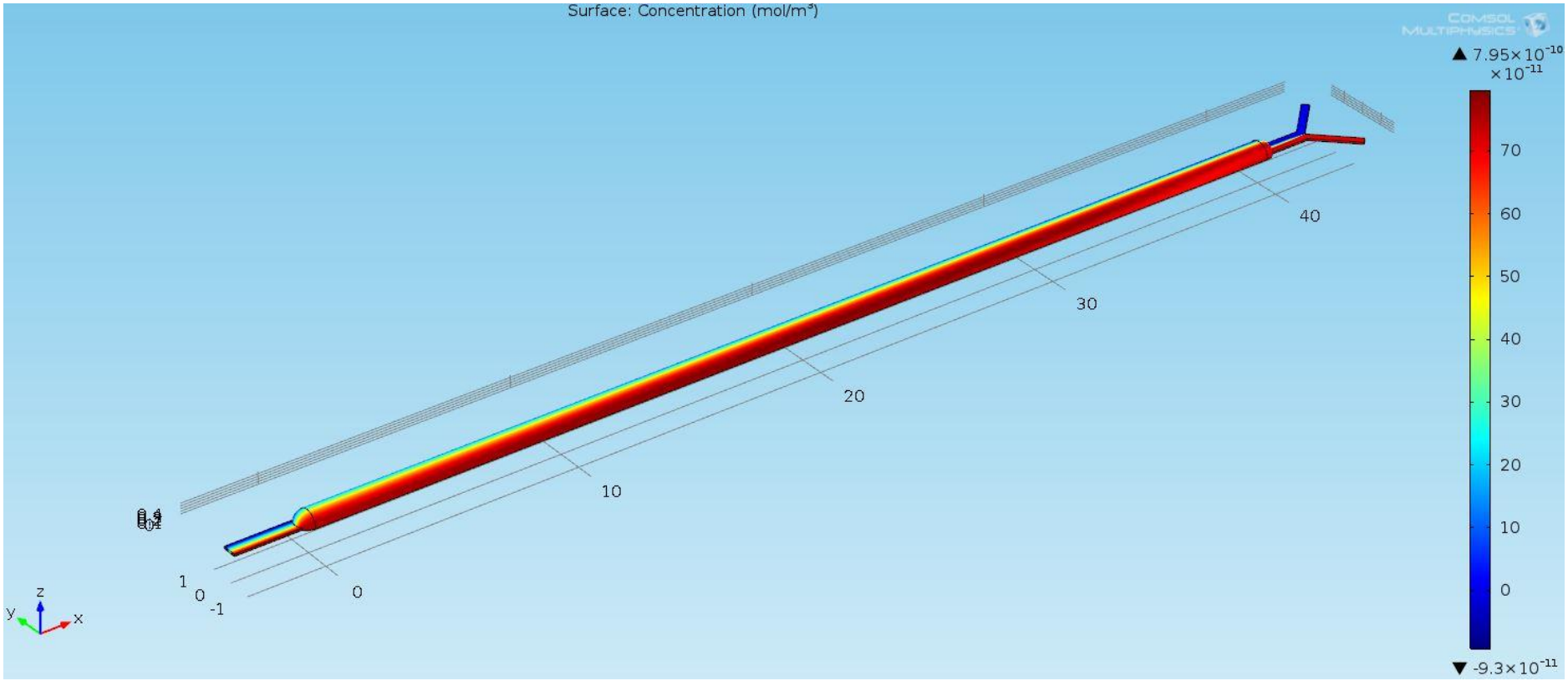

Figure A-2. *Isometric view of the mixing in the T-junction micromixer*

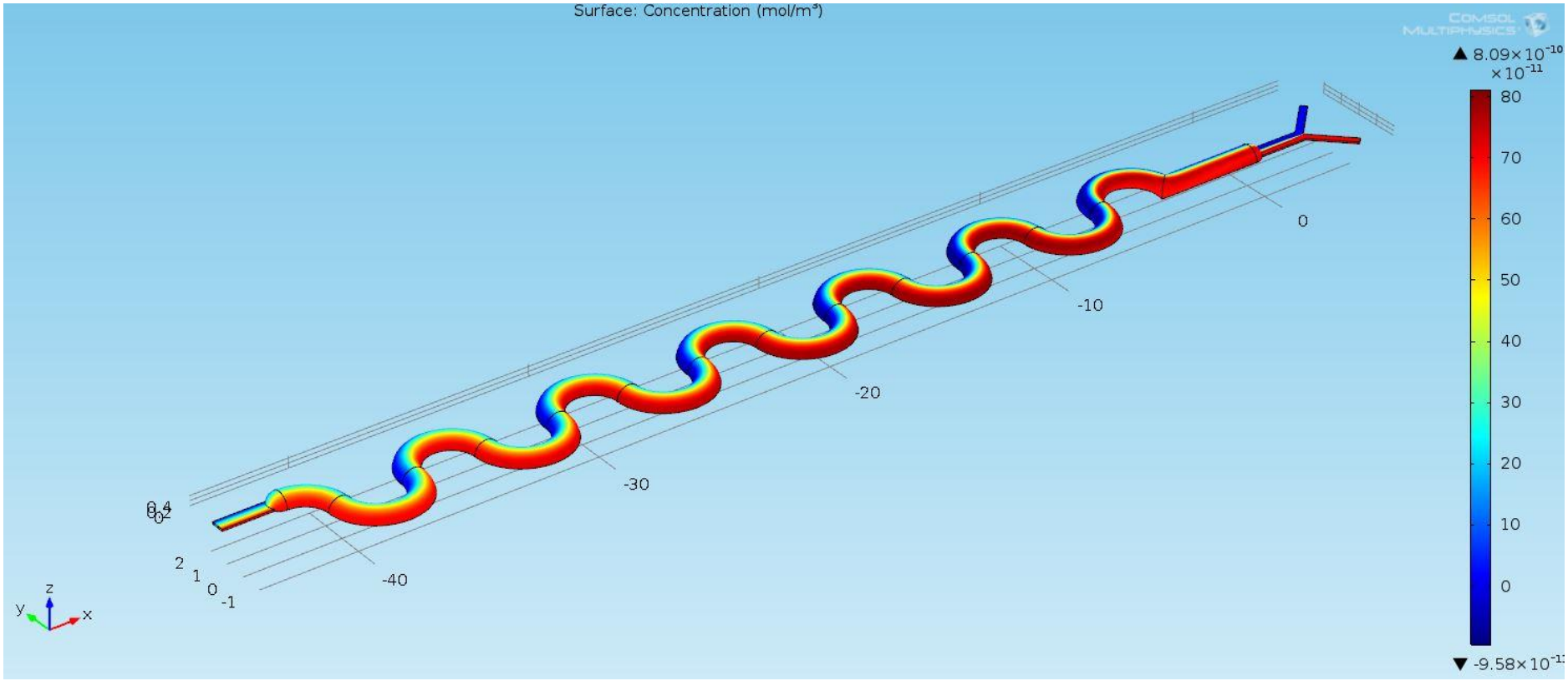

Figure A-3. *Isometric view of the mixing in the Serpentine micromixer.*

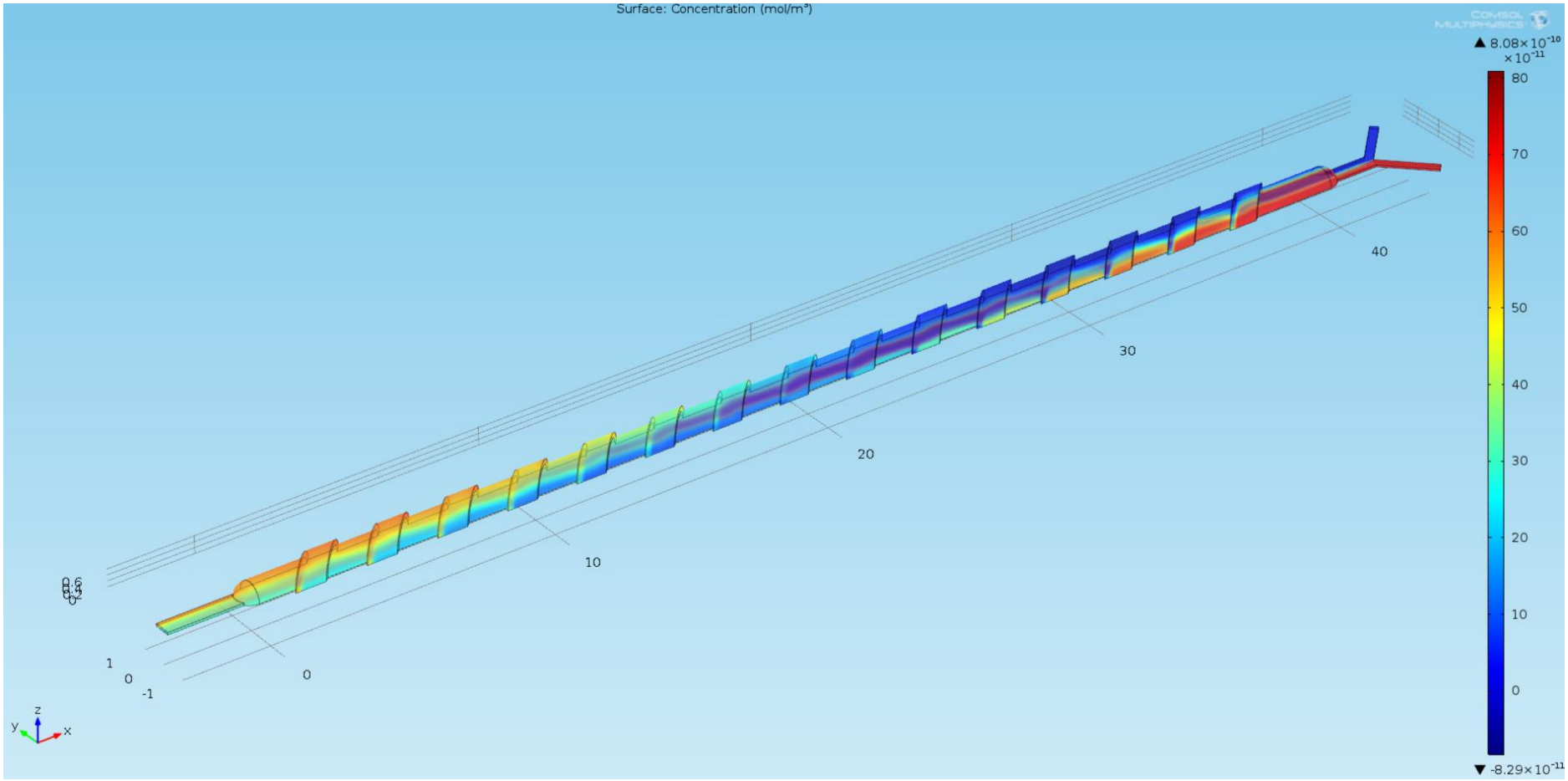

Figure A-4. *Isometric view of the mixing in the grooves micromixer. Here the transparency was enabled in COMSOL in order to better view the mixing behavior.*

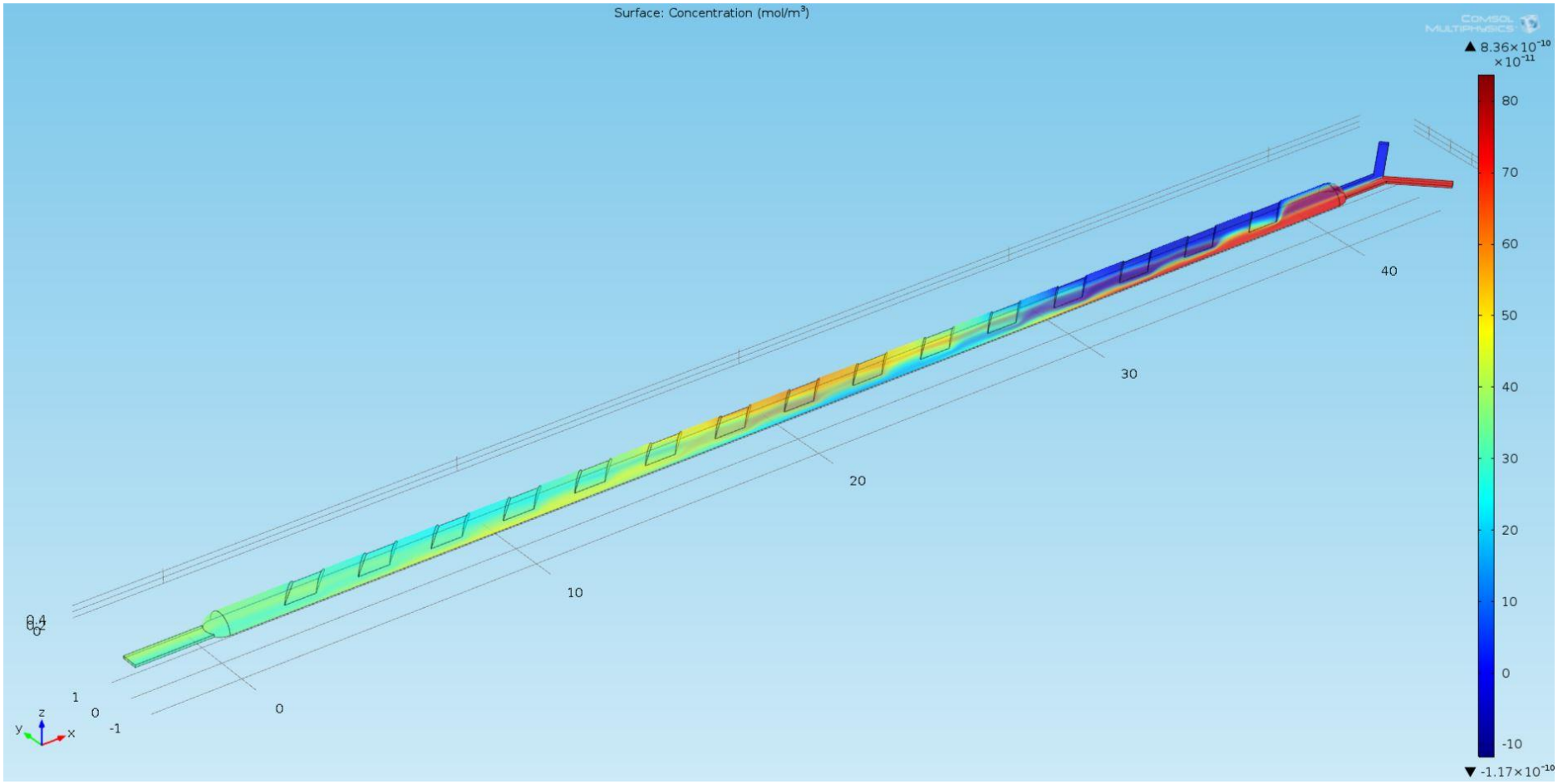

Figure A-5. *Isometric view of the mixing in the slanted rips micromixer. Here the transparency was enabled in COMSOL in order to better view the mixing behavior.*

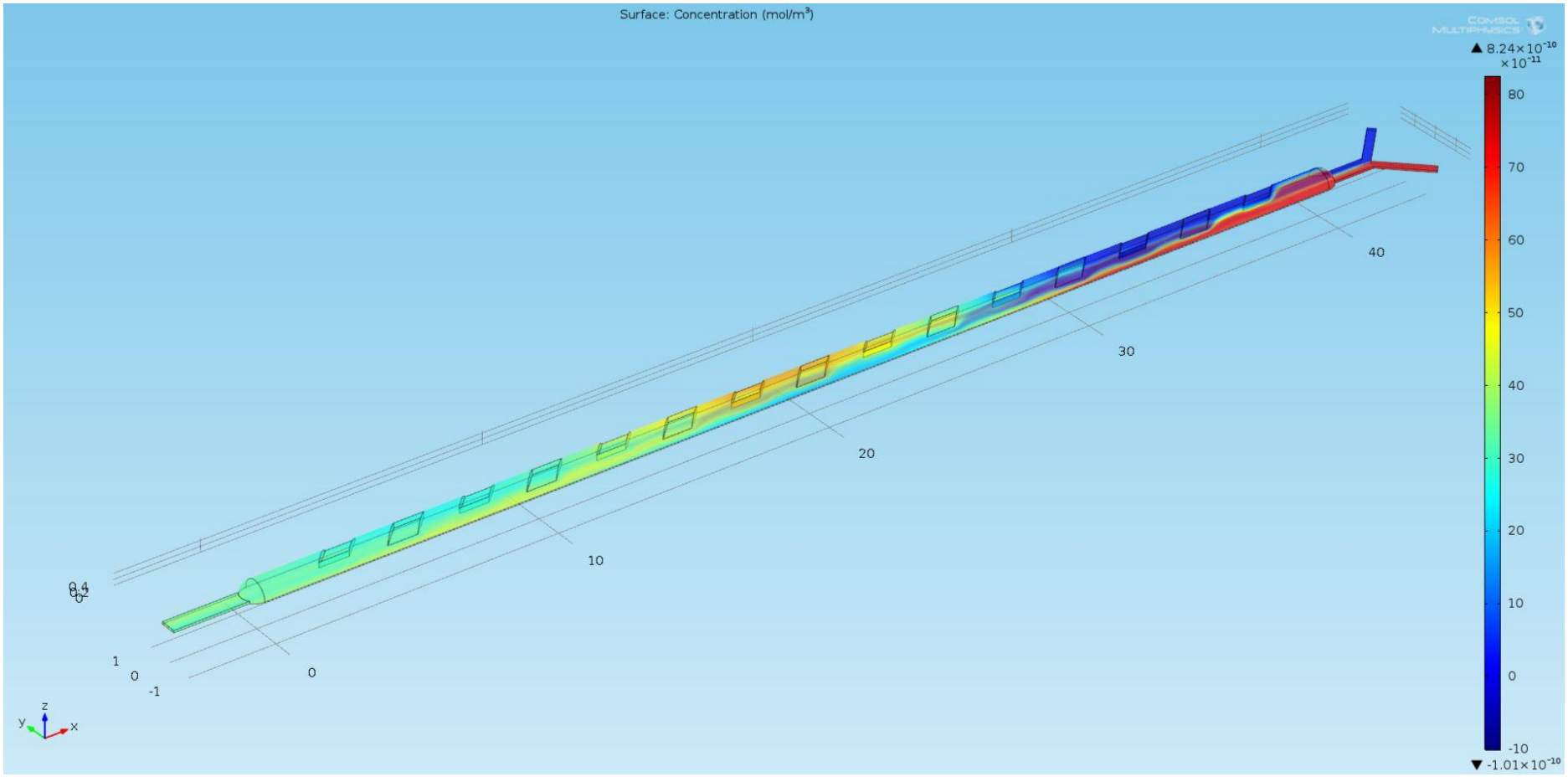

Figure A-6. *Isometric view of the mixing in the modified slanted rips micromixer. Here the transparency was enabled in COMSOL in order to better view the mixing behavior.*

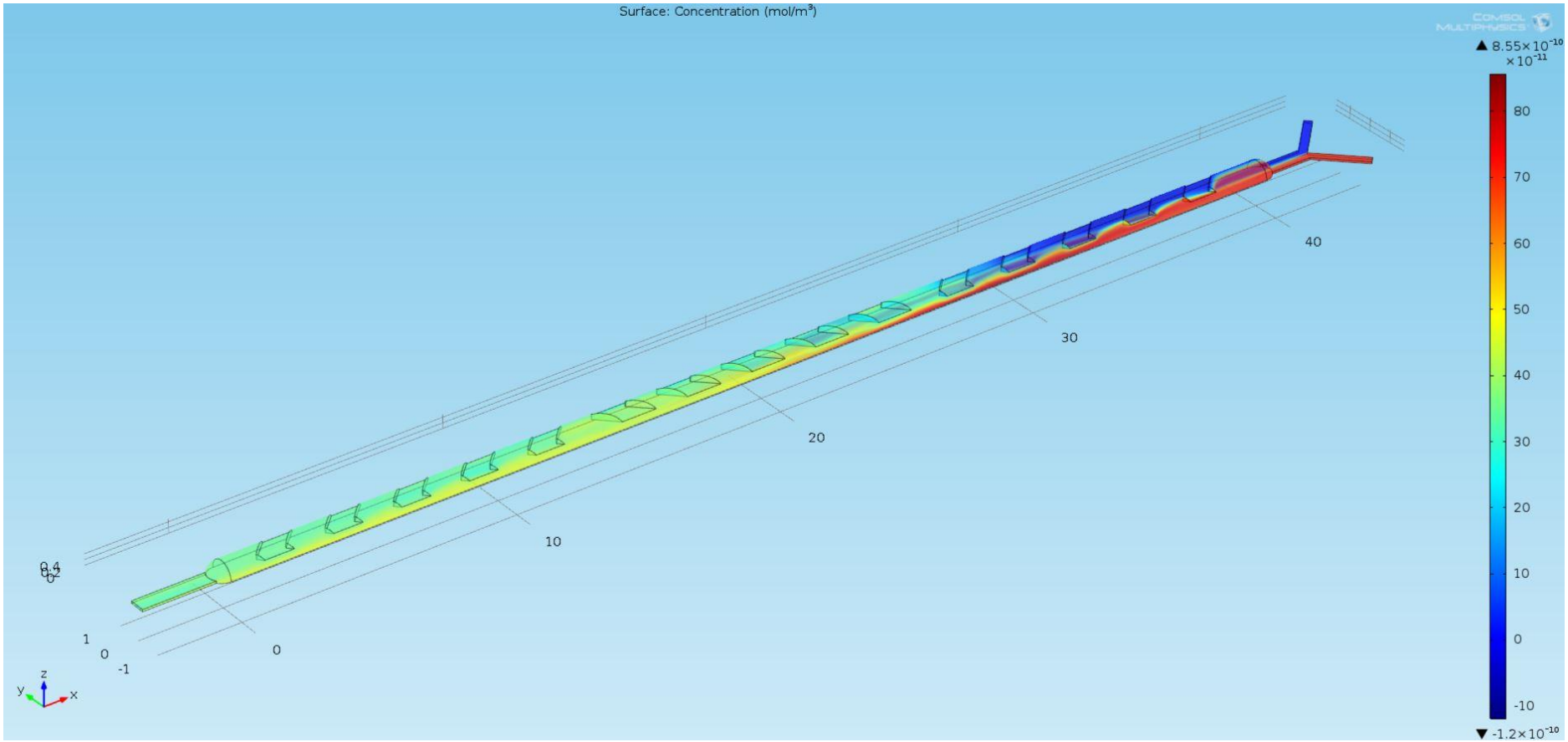

Figure A-7. *Isometric view of the mixing in the staggered herringbone micromixer. Here the transparency was enabled in COMSOL in order to better view the mixing behavior.*

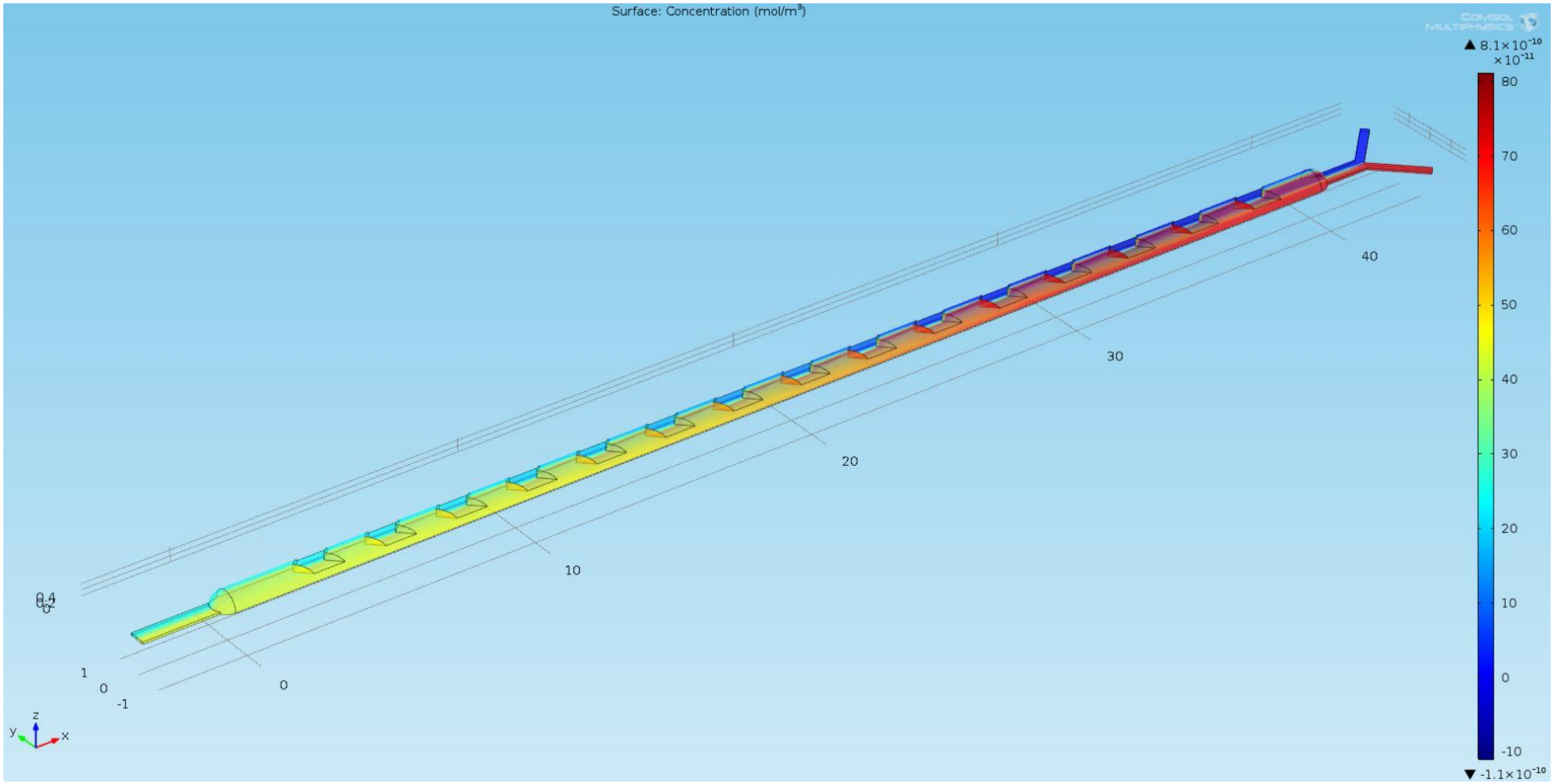

Figure A-8. *Isometric view of the mixing in the modified staggered herringbone micromixer. Here the transparency was enabled in COMSOL in order to better view the mixing behavior.*

APPENDIX B: XY AND XZ SLICES OF VARIOUS CHAOTIC ADVECTION MICROMIXERS

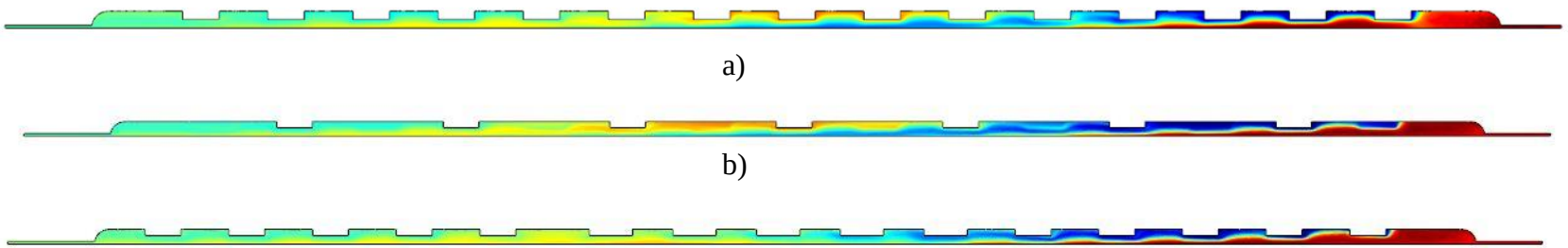

a)

b)

c)

Figure B-1. *xz plane slice at y=-2.5 mm of a) slanted rips, b) modified slanted rips, c) herringbone structures.*

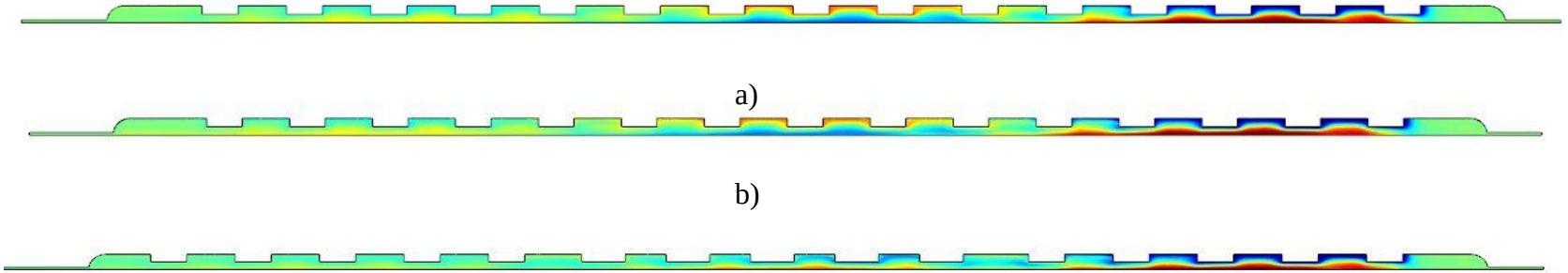

a)

b)

c)

Figure B-2. *xz plane slice at y=0 mm of a) slanted rips, b) modified slanted rips, c) herringbone structures.*

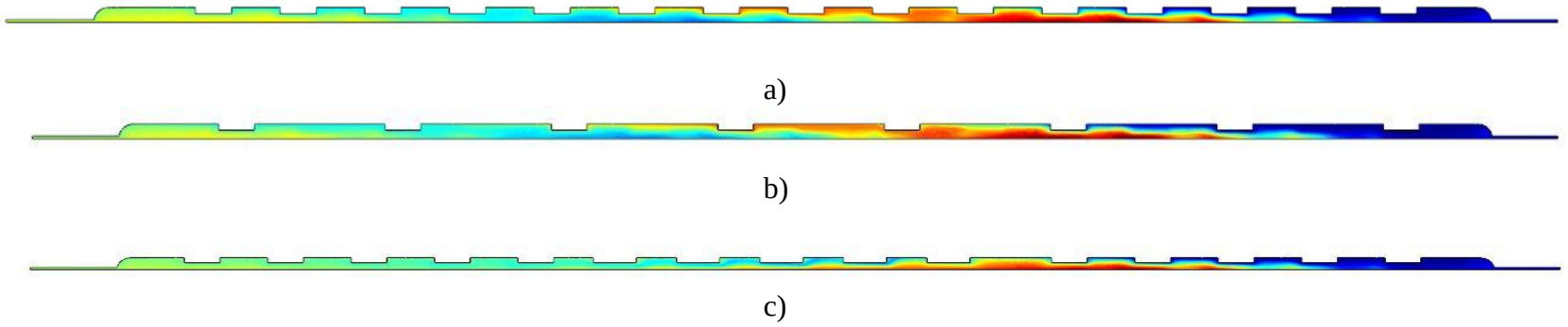

a)

b)

c)

Figure B-3. *xz plane slice at y=2.5 mm of a) slanted rips, b) modified slanted rips, c) herringbone structures.*

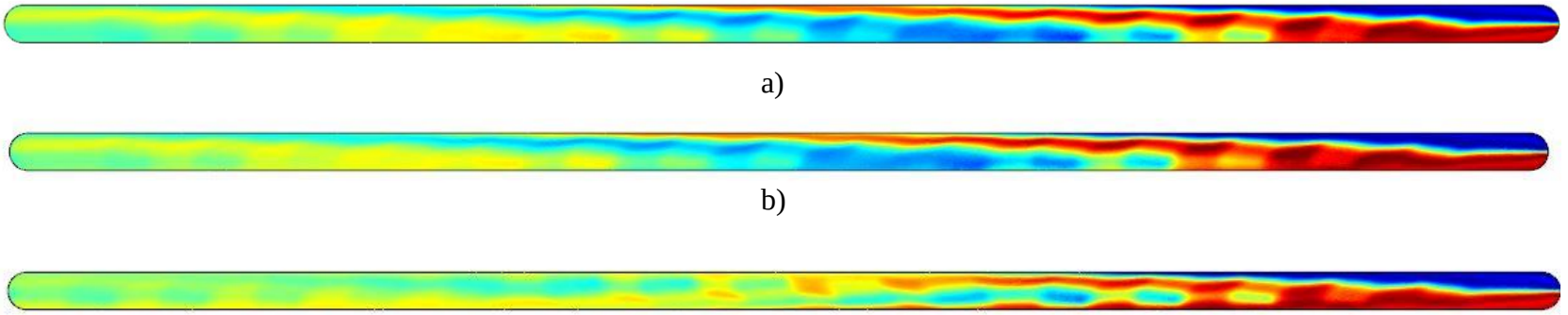

a)

b)

c)

Figure B-4. *xy plane slice at z=0.1 mm of a) slanted rips, b) modified slanted rips, c) herringbone structures.*

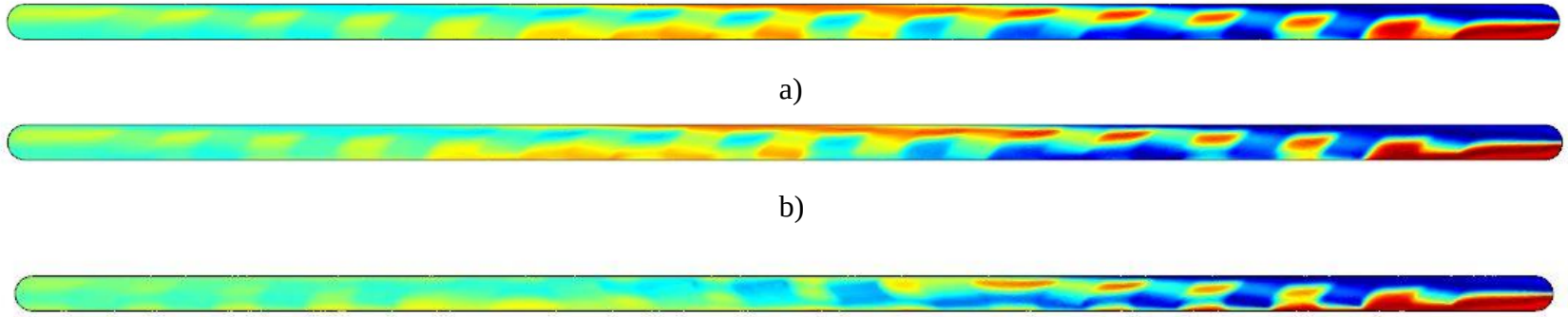

Figure B-5. *xy plane slice at z=0.3 mm of a) slanted rips, b) modified slanted rips, c) herringbone structures.*

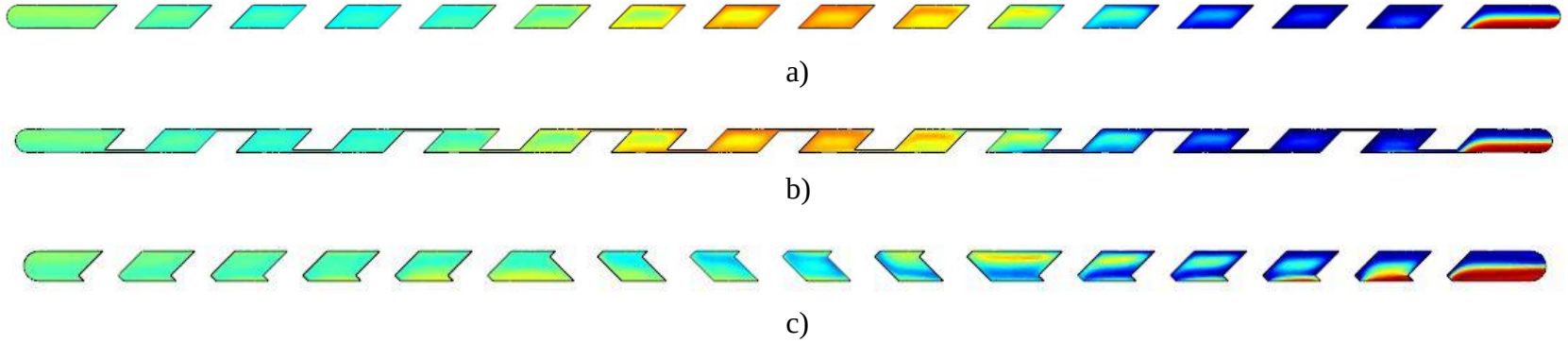

Figure B-6. *xy plane slice at z=0.4 mm of a) slanted rips, b) modified slanted rips, c) herringbone structure*